



## Ice thickness and bed topography of Jostedalsbreen ice cap, Norway

Mette K. Gillespie<sup>1</sup>, Liss M. Andreassen<sup>2</sup>, Matthias Huss<sup>3,4,5</sup>, Simon de Villiers<sup>1</sup>, Kamilla H. Sjursen<sup>1</sup>, Jostein Aasen<sup>2</sup>, Jostein Bakke<sup>6</sup>, Jan M. Cederstrøm<sup>6</sup>, Hallgeir Elvehøy<sup>2</sup>, Bjarne Kjøllmoen<sup>2</sup>, Even Loe<sup>7</sup>, Marte Meland<sup>8</sup>, Kjetil Melvold<sup>2</sup>, Sigurd D. Nerhus<sup>1</sup>, Torgeir O. Røthe<sup>1</sup>, Eivind W. N. Støren<sup>6,9</sup>, Kåre Øst<sup>10</sup>, Jacob C. Yde<sup>1</sup>

<sup>1</sup>Department of Civil Engineering and Environmental Sciences, Western Norway University of Applied Sciences, Sogndal, 6851, Norway

<sup>2</sup>Section for Glaciers, Ice and Snow, Norwegian Water Resources and Energy Directorate (NVE), Oslo, 0301, Norway

<sup>3</sup>Laboratory of Hydraulics, Hydrology and Glaciology (VAW), ETH Zurich, Zurich, 8092, Switzerland

<sup>4</sup>Swiss Federal Institute for Forest, Snow and Landscape Research (WSL), Birmensdorf, CH-8903, Switzerland

<sup>5</sup>Department of Geosciences, University of Fribourg, Fribourg, 1700, Switzerland

<sup>6</sup>Department of Earth Science and the Bjerknes Centre for Climate Research, University of Bergen, 5020, Norway

<sup>7</sup>Statkraft, Gaupne, 6868, Norway

<sup>8</sup>Breheimsenteret, Jostedal, 6871, Norway

<sup>9</sup>COWI, Bergen, 5824, Norway

<sup>10</sup>Norgesguidene, Jostedal, 6871, Norway

*Correspondence to:* Mette Kusk Gillespie (mette.kusk.gillespie@hvl.no)

**Abstract.** We present an extensive dataset of ice thickness measurements from Jostedalsbreen ice cap, mainland Europe's largest glacier. The dataset consists of more than 351 000 point values of ice thickness distributed along ~1100 km profile segments that cover most of the ice cap. Ice thickness was measured during field campaigns in 2018, 2021, 2022, and 2023 using various ground-penetrating radar (GPR) systems with frequencies ranging between 2.5 and 500 MHz. The large majority of ice thickness observations were collected in spring using either snowmobiles (90 %) or a helicopter-based radar system (8 %), while summer measurements were carried out on foot (2 %). To ensure accessibility and ease of use, metadata were attributed following the GlaThiDa dataset and follows the FAIR (Findable, Accessible, Interoperable, and Reusable) guiding principles. Our findings show that glacier ice of more than 400 m thickness is found in the upper regions of large outlet glaciers, with a maximum ice thickness of ~630 m in the Tunsbergdalsbreen outlet glacier accumulation area. Thin ice of less than 50 m covers narrow regions joining the central part of Jostedalsbreen with its northern and southern parts, making the ice cap vulnerable to break-up with future climate warming. Using the point values of ice thickness as input to an ice thickness model, we compute 10 m grids of ice thickness and bed topography that cover the entire ice cap. From these distributed datasets we find that Jostedalsbreen has a mean ice thickness of 154 m  $\pm$  22 m and a present (~2020) ice volume of 70.6  $\pm$  10.2 km<sup>3</sup>. Locations of depressions in the map of bed topography are used to delimitate the locations of potential future lakes, consequently providing a glimpse of the landscape if the entire



Jostedalsgreen melts away. Together, the comprehensive ice thickness point values and ice cap-wide grids serve as a baseline for future climate change impact studies at Jostedalsgreen.

All data are available for download at <https://doi.org/10.58059/yhwr-rx55> (Gillespie et al., 2024).

## 1 Introduction

40 Global glacier mass loss caused by increased atmospheric temperatures contributes significantly to changes in sea level, water resources and natural hazards (IPCC, 2021). Projections of future changes show that glaciers and ice caps will continue to lose mass due to anthropogenic warming, and that the majority of the world's glaciers and ice caps are at risk of being lost by 2100 (Rounce et al., 2023). However, global glacier projections remain uncertain. This is especially true for ice caps, where model efforts of ice thickness distribution in the flat upper  
45 regions and across ice divides represents a particular challenge (Millan et al., 2022; Frank et al., 2023).

Information on ice thickness distribution of a glacier is a prerequisite for accurate modelling of ice dynamics and glacier evolution, as well as future hydrological impacts. Ice thickness measurements are also essential for precise calculations of the ice volume of glaciers and in mapping of the subglacial topography. Consequently, significant  
50 efforts have been made to compile ice thickness data and provide grids of ice thickness and bed topography (e.g., Gärtner-Roer et al., 2014; Lindbäck et al., 2018; Frémand et al., 2023). The third version of the Glacier Thickness Database (GlaThiDa v3) includes nearly 4 million ice thickness measurements distributed over roughly 3000 glaciers worldwide, and 14 % of the world's glacierized area is now within 1 km of an ice thickness measurement (GlaThiDa Consortium, 2020; Welty et al., 2020). Direct inter- and extrapolation of ice thickness measurements  
55 with various techniques, such as kriging, inverse-distance weighting, or spline interpolations (Flowers and Clarke, 1999; Binder et al., 2009; Fischer, 2009; Yde et al., 2014; Andreassen et al., 2015) is possible, but may produce large uncertainties in areas without measurements (Gillespie et al., 2023). Consequently, ice thickness modelling is necessary to extrapolate measurements more accurately to unmeasured regions (Andreassen et al., 2015; Farinotti et al., 2021), and to infer ice thickness for glaciers without direct measurements.

60 Various ice thickness inversion approaches exist that do not require bed topography or ice thickness as input (e.g., Huss and Farinotti et al., 2012; Linsbauer et al., 2012; Fürst et al., 2017; Farinotti et al., 2019; Frank et al., 2023), and recent efforts to model ice thickness through inversion of surface topography have made distributed ice thickness information available for every individual glacier in the world (Farinotti et al., 2019; Millan et al., 2022) and  
65 all Scandinavian glaciers and ice caps (Frank and van Pelt, 2024). Although ice thickness observations are not required as input in these models, databases of ice thickness, when available, remain important for calibration and validation of model behaviour. Assessments of model performances, such as the first Ice Thickness Model



Intercomparison eXperiment (ITMIX; Farinotti et al., 2017), found that model output is highly variable, and that the best results are achieved when using model ensembles. In addition, a more recent model comparison (ITMIX2; 70 Farinotti et al., 2021) demonstrated the added value of in situ ice thickness observations to constrain models. A limited set of ice thickness observations, preferably from the thickest parts of the glacier, provided efficient in constraining mean glacier thickness, illustrating that even sparse ice thickness observations are of importance in ice thickness modelling. Consequently, readily accessible ice thickness observations for calibration and validation remains key for developing a new generation of ice thickness estimation models (Farinotti et al., 2017). 75 Measurements across the flat upper regions of ice caps such as Jostedalbreen are of particular value, as these can be applied to improve ice thickness models for the much larger ice sheets in Greenland and Antarctica, and ultimately facilitate more accurate predictions of future sea-level change (Morlighem et al., 2017).

In Norway, numerous field campaigns to measure ice thickness have been carried out over the years (Andreassen 80 et al., 2015). The purpose of the earliest measurements was typically to determine subglacial topography in relation to hydropower planning, such as subglacial intakes and water divides (e.g., Kennett, 1989; 1990), or detailed studies related to jökulhlaups (Engeset et al., 2005). While the first attempts at ice thickness mapping used seismic measurements (e.g., Sellevoid and Kloster, 1964) or hot water drilling (e.g., Østrem et al., 1976), from 1980 ground-penetrating radar (GPR) has been the preferred method for largescale mapping of glaciers in Norway (e.g., 85 Sætrang and Wold, 1986). Since these first radar measurements on Norwegian glaciers, technological advancements in radar systems, processing techniques and positioning accuracy have enabled the use of GPR in a wide range of glaciological applications, such as mapping of ice- or snow thickness, internal layering, thermal regime, or englacial meltwater channels (e.g., Plewes and Hubbard, 2001; Dowdeswell and Evans, 2004; Navarro and Eisen, 2009). The penetration depth and level of detail in GPR data are determined by the antenna frequency. 90 Information on ice and snow characteristics can be achieved by using very-high (30–300 MHz) or ultra-high (300–3000 MHz) antenna frequencies, while high-frequency GPR surveys (3–30 MHz antenna frequency) have larger penetration depth at the expense of resolution (Schlegel et al., 2022). High-frequency antennas are consequently the better choice in surveys of bed topography and grids of glacier geometry based on such measurements have been widely used to model future changes in Norwegian glaciers (e.g., Laumann and Nesje, 2009, 2014; Giesen 95 et al., 2010; Åkesson et al., 2017, Johansson et al., 2022).

Jostedalbreen is the largest ice cap in mainland Europe and makes up about 20 % of the total glacierized area of mainland Norway (Andreassen et al., 2022). The effect of global warming is evident in the region and monitored outlet glaciers flowing from the ice cap have thinned and retreated with increased speed since 2000 (e.g., 100 Andreassen et al., 2020; Seier et al., 2024). The effects of future warming on accessibility, glacier-atmosphere systems and hydrology are likely to significantly impact regional businesses such as agriculture, tourism, and



hydropower production. Despite the importance of Jostedalbreen to both regional stakeholders and the scientific community, the natural and societal consequences of climate-forced changes in the region remain largely unknown. Future changes of Jostedalbreen can be assessed through glacier evolution modelling, but accurate results  
105 require high-quality information on ice thickness and bed topography as model input (Farinotti et al., 2017). Although several surveys of ice thickness were conducted on Jostedalbreen during the 1970s and 1980s (e.g., Østrem et al., 1976; Andreassen et al., 2015), prior to the new ice thickness measurements described in this paper, many parts of the ice cap had either poor or no data coverage.

110 Here we present a comprehensive and up-to-date point dataset of ice thicknesses of Jostedalbreen measured by GPR during the period 2018–2023. Ice thickness measurements were predominantly performed on the glacier surface (ground-based), but in regions that were inaccessible on the ground we applied a helicopter (airborne) radar system. We used antenna frequencies ranging from 2.5 to 500 MHz to capture the thickness of the ice in the best possible resolution. For regions that remain unmeasured due to resource or accessibility constraints, we use  
115 interpolation and ice thickness modelling to provide new grids of ice thickness and bed topography for the entire ice cap. Depressions in the subglacial bed topography grid are used to infer the locations of lakes if Jostedalbreen disappeared completely from the landscape. We provide a thorough description of the uncertainties associated with ice thickness measurements and modelling results, including comprehensive uncertainty estimates. The enhanced datasets on Jostedalbreen ice thickness and bed topography have the potential to significantly advance  
120 modelling efforts for the past and future evolution of the ice cap and provide accurate assessments of regional climate change impact. In addition, comprehensive high-accuracy measurements over the complex glacier geometry at Jostedalbreen constitute a valuable resource for improving current ice thickness models, particularly on ice caps, where the flat upper regions and discontinuities across ice divides provide a special challenge.

## 2 Study site

125 Jostedalbreen (Fig. 1) has an area of 458 km<sup>2</sup> and an elevation ranging between 380 and 2006 m a.s.l. (Andreassen et al., 2022). The climate is subarctic to tundra with a mean annual air temperature of -3°C at 1633 m a.s.l. (2009–2022 average at Steinmannen meteorological station; Engen et al., in review). In the most recent national glacier inventory, Jostedalbreen is divided into 81 glacier units from observations of topographic ice divides (Andreassen et al., 2022). Many of these glacier units have individual names which will be referred to  
130 throughout this paper. Jostedalbreen is defined as a single ice cap but can geographically be divided into three minor ice caps that are currently connected (Fig. 1). In this paper, we refer to Jostedalbreen South (south of Grensevarden), Central (north of Grensevarden as far as and including Lodalsbreen glacier) and North (northeast of Lodalsbreen glacier).



135 Jostedalsbreen reached its maximum Little Ice Age (LIA) extent between 1740 and 1860 CE with an estimated  
area of 572 km<sup>2</sup> (Carrivick et al., 2022; Andreassen et al., 2023). Since then, the ice cap has experienced an overall  
reduction in size, interrupted temporarily by advances in several fast-responding outlet glaciers, the latest of which  
occurred in the 1990s due to increased winter precipitation (Nesje et al., 1995; Andreassen et al., 2005). By 2006,  
the major outlet glaciers had in combination lost at least 93 km<sup>2</sup> or 16 % of their LIA area and 14 km<sup>3</sup> or 18 % of  
140 their LIA volume (Carrivick et al., 2022). Increasing summer temperatures further reduced the glacier area by 3 %  
from 2006 to 2019 (Andreassen et al., 2022) and continues to this day (Seier et al. 2024). Overall, the change in  
the glacial landscape has been considerable, with measurements of glacier front variation (length changes) at  
several outlet glaciers revealing a total reduction in length of 1–3 km since ~1900 (Andreassen et al., 2023), of  
which 300–700 m has occurred since 2000 (Kjøllmoen et al., in prep.).

145

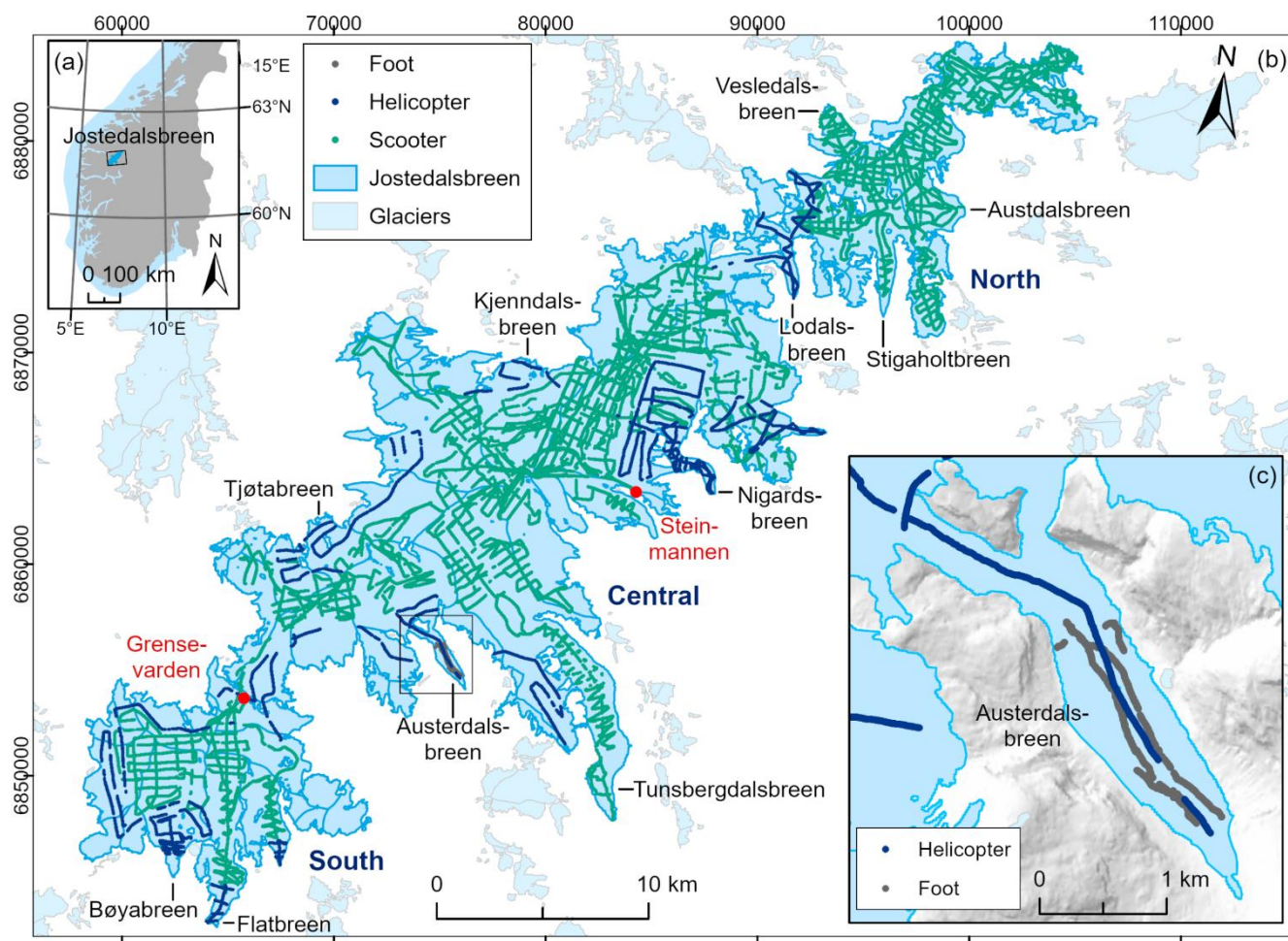
The first ice thickness measurements on Jostedalsbreen were conducted in 1973 along two cross profiles located  
between 700 and 800 m a.s.l. on the tongue of Nigardsbreen outlet glacier (Østrem et al., 1976). In total, 14 points  
were drilled using electrical hot-point drilling, revealing ice thicknesses of up to 200 m. In 1986 hot water drilling  
was carried out on Bødalsbreen outlet glacier along three cross profiles at 780–815 m a.s.l. (Haakensen and Wold,  
150 1986). Results from 15 boreholes show that ice thickness varied between 50 and 60 m in this region. GPR was  
first used on Jostedalsbreen in the 1980s during field campaigns on Nigardsbreen and surrounding glaciers in  
1981, 1984, and 1985 (Sætrang and Wold, 1986), on Austdalsbreen and surrounding glaciers in 1986 (Sætrang  
and Holmqvist, 1987), and south of Nigardsbreen in 1989 (Andreassen et al., 2015). Results show that ice thickness  
along transects typically varied between 150 and 300 m, with ice of up to 600 m in the flattest regions and thinner  
155 ice (50–100 m) at the highest points of the ice cap (Sætrang and Wold, 1986). These early measurements of ice  
thickness are associated with relatively large uncertainties in surface elevations and the positioning of GPR profiles.  
In addition, as data were collected and processed with analogue techniques, only parts of the older dataset are  
available digitally. Digitised data from these campaigns have been submitted to the GlaThiDa database (GlaThiDa  
Consortium, 2020; Welty et al., 2020) and were used by Andreassen et al. (2015) to interpolate ice thickness  
160 distribution and estimate a mean ice thickness of 158 m for parts of Jostedalsbreen (65 % of total area). More  
recently, Jostedalsbreen was included in a modelling study of ice volume and thickness distribution of all  
Scandinavian glaciers (Frank and van Pelt, 2024). In this study, existing ice thickness measurements were used  
to calibrate an ice thicknesses model, resulting in a total volume of 72.6 km<sup>3</sup> for Jostedalsbreen.



### 3 Methods and data

#### 165 3.1 Ice thickness measurements

The ice thickness measurements presented in this paper were collected during field campaigns between 2018 and 2023. The first measurements were carried out in April 2018, however most of the data were gathered in April 2021, March to April 2022 and April 2023 (Fig. A1), while the tongue of Austerdalsbreen was surveyed in September 2021. The principle means of transport during data collection was snowmobile (90 % of all datapoints), but a newly  
170 developed helicopter radar system (Air-IPR) was deployed in steep and crevassed regions of the ice cap (8 % of all datapoints). Summer measurements on foot account for only 2 % of all datapoints (Fig. 2). Although airborne surveys were quicker, ground-based measurements were preferred whenever possible due to the generally better data quality caused by lower travel speeds, less noise (electronic and off nadir-reflections) and simpler wave propagation (lack of an air layer). Depending on the surface conditions, we collected the data in a grid pattern, with  
175 the main profiles spaced no more than 400 m apart and oriented transverse to the ice flow direction. Survey lines perpendicular to main profiles were 400–800 m apart, depending on accessibility and time constrains during the fieldwork. In total, we have successfully detected the glacier bed along ~920 km of profile segments collected with the ground-based radar systems and ~170 km of profile segments collected with the airborne radar system (Fig. 1). Following the new measurements, 90 % of the ice cap is now less than 300 m from an observation of ice  
180 thickness (measurement or glacier outline) and 49 % is within 100 m of a known point.



185 **Figure 1: Map showing (a) the location of Jostedalsgreen in southern Norway, (b) Jostedalsgreen and GPR surveys divided into helicopter, snowmobile, and foot, and (c) the measurements on Austerdalsgreen by foot and helicopter. The shown glacier extent and outline of glacier units are from 2019 (Andreassen et al., 2022). Background mountain shadow on (c) is from the 100 m national DTM by the Norwegian Mapping Authority. The coordinate systems are geographical coordinates on (a) and UTM 33N, datum ETRS89 on (b) and (c).**

Based on the terminology proposed by Schlegel et al. (2023), we used a combination of high, very high and ultra-  
190 high frequency radar systems to gather detailed information on snow, firn and shallow ice, while maintaining a good penetration depth for deep ice. Usually two snowmobiles would travel together, one towing a high frequency generation 1–3 Blue System Integration Ltd. IceRadar system with 2.5 or 5 MHz antennas (Mingo and Flowers, 2010) depending on the ice thickness in the investigated area, and the other snowmobile towing either a higher frequency Malå GPR system with 25 or 50 MHz rough terrain antennas, or 450 or 500 MHz shielded antennas  
195 (Table 1). On one occasion, measurements were conducted using a Radarteam GPR system with a 40 MHz monostatic antenna and an upgraded non-commercial GPR with 5 MHz antennas (NVE-radar), similar to that



described by Sverrisson et al. (1980) and Pettersson et al. (2011). For the measurements on foot on the tongue of Austerdalsbreen, we chose a 10 MHz Blue System Integration Ltd. IceRadar and a 50 MHz Malå GPR. All helicopter measurements were collected using a 5 MHz Air-IPR Generation 3 Blue System Integration Ltd. IceRadar system with the antennas in a V dipole configuration (Table 1). The carrying platform for the Air-IPR is built with wood and uses telescopic rods in composite material to hold the antennas (Fig. 2c). To secure an accurate distance between the antennas and the ice surface, we used a laser mounted on the platform with a wireless connection to the cockpit. The control of the IceRadar during both ground-based and airborne measurements was performed using a tablet and a remote connection.

205



**Figure 2: Data collection was undertaken (a) by snowmobile, (b) on foot, and (c) by helicopter. Photos: (a) Kjetil Melvold, (b) Mette K. Gillespie and (c) Torgeir O. Røthe.**

210 Ground-based measurements of ice thickness were largely carried out using an in-line antenna configuration with distances between receiver (Rx) and transmitter (Tx) units depending on the antenna frequency, and varying from 4 m (50 MHz) and 6.5 m (25 MHz) for the two Malå rough terrain antennas to 15 m (10 MHz), 30 m (5 MHz) and 60 m (2.5 MHz) for the three IceRadar antenna sets. The 5 MHz NVE-radar antennas were also run using an in-line configuration, but with 32 m between antenna mid-points. By contrast, the shielded 450 MHz and 500 MHz  
215 Malå antennas were oriented perpendicular to the travel direction and with a 0.18 m antenna separation. To avoid interference between radar systems during data collection, the two snowmobiles travelled at a distance of more than 50 m. For frequencies of 25 MHz and above, each measurement (trace) was stacked between 4 and 8 times to increase the signal-to-noise ratio, whereas the 2.5 and 5 MHz measurements were stacked 256 times. Ice thickness measurements were collected at a constant time interval, which varied according to limitations in the  
220 different radar systems. The distance between individual traces along radar profiles was affected by this and our travel speed ( $\sim 15 \text{ km h}^{-1}$ ). Measurements collected with antenna frequencies ranging between 25 and 500 MHz





were sampled at the highest rate (trace distances of ~0.2–2 m). Therefore, while these measurements constitute a significant proportion of total datapoints (Table 1), the vast majority of data coverage is attributed to ice thickness observations along 5 and 2.5 MHz profiles, which were collected less densely. In general, ground-based measurements of ice thickness were registered at intervals ranging between 3 and 6 m, while airborne measurements were 3 to 20 m apart.

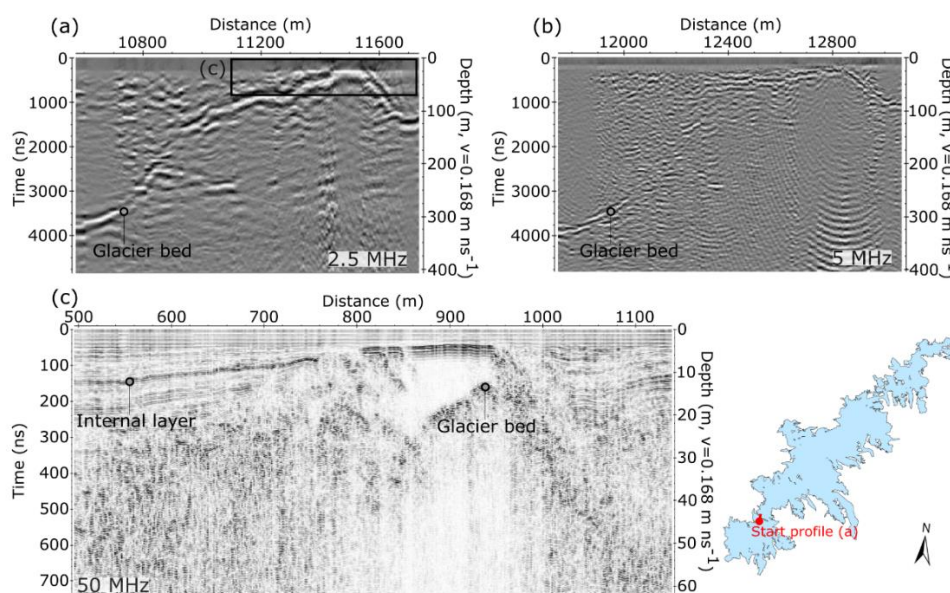
GNSS locations along survey lines were recorded every 1 s with a horizontal positioning accuracy of up to 5 m for the Malå radar system (G-Star IV BU-353S4 receiver) and 3 m for the IceRadar system (Garmin GPSx OEM sensor). In addition, differential GNSS (DGNSS) measurements were carried out independently of the radar measurements in some regions.

**Table 1: Survey dates and equipment used for ice thickness measurements during the 2018–2023 field campaigns. The number of datapoints refers to the post-processed and interpreted dataset. Institutions are Western Norway University of Applied Sciences (HVL), the Norwegian Water Resources and Energy Directorate (NVE) and University of Bergen (UIB).**

Method	Radar type	Frequency	Points	Survey dates	Institutions
<i>Ground-based radar</i>	IceRadar	2.5 MHz	15712	18–19 April 2018	HVL
	NVE-radar	5 MHz	18569	18 April 2018	NVE
	IceRadar Malå GPR Malå GPR	2.5 and 5 MHz 50 MHz RTA 450 MHz shielded	99745 4503 15308	11–18 April 2021	HVL
	RadarTeam Subecho 40	40 MHz	32533	16–17 April 2021	NVE
	IceRadar Malå GPR	2.5 MHz 25 MHz RTA	5221 5753	20–24 April 2021	UIB
	IceRadar Malå GPR	10 MHz 50 MHz RTA	4825 2723	4 September 2021	HVL
	IceRadar	5 MHz	11769	8 March 2022	HVL
	IceRadar Malå GPR	5 MHz 25 and 50 MHz RTA	18424 11938	19–22 March 2022	HVL
	IceRadar	5 MHz	5856	5–6 April 2022	NVE
	IceRadar Malå GPR Malå GPR	5 MHz 50 MHz RTA 500 MHz shielded	53061 12509 4282	20–21 April 2022	HVL
<i>Airborne radar</i>	IceRadar	2.5 MHz	621	22 March 2023	HVL
	IceRadar	5 MHz	5725	22 March 2022	UIB
	IceRadar	5 MHz	5151	7 April 2022	UIB and HVL
	IceRadar	5 MHz	5267	26 April 2022	HVL
	IceRadar	5 MHz	12064	20 April 2023	HVL

### 3.2 Data processing and interpretation

The raw GPR data was primarily processed using the ReflexW module for 2D data analysis (Sandmeier Scientific Software, version 8.5). Initial data processing involved adding GNSS positions for antenna midpoints to all traces, merging individual shorter profiles into larger segments, and assigning a constant trace increment along each segment to allow for subsequent migration. We chose a trace increment close to the mean value during travel to avoid deleting or introducing too many traces to the original dataset. Following the initial data sorting, we used a combination of 1) dewow, 2) Butterworth bandpass filtering, 3) time zero correction, 4) dynamic correction, 5) energy decay gain, and 6) f-k Stolt migration on all ground-based measurements. For the GPR measurements collected with 2.5 and 5 MHz systems, processing steps 3) and 4) are important to account for the influence of the large antenna separation on first signal arrival times and the radar wave path through the ice. Further filtering was required on the airborne measurements due to significant system-related noise. The processing routine for this portion of the dataset consequently involved applying an adaptive filter using the IceRadarAnalyzer processing software (Blue System Integration Ltd., version 6.3.1. beta) to remove unwanted signals from the radar profiles, in addition to dewow and bandpass filtering. Subsequent static correction was undertaken in ReflexW using manually delineated arrival times of the glacier surface reflection, after which energy decay gain and f-k Stolt migration were applied.

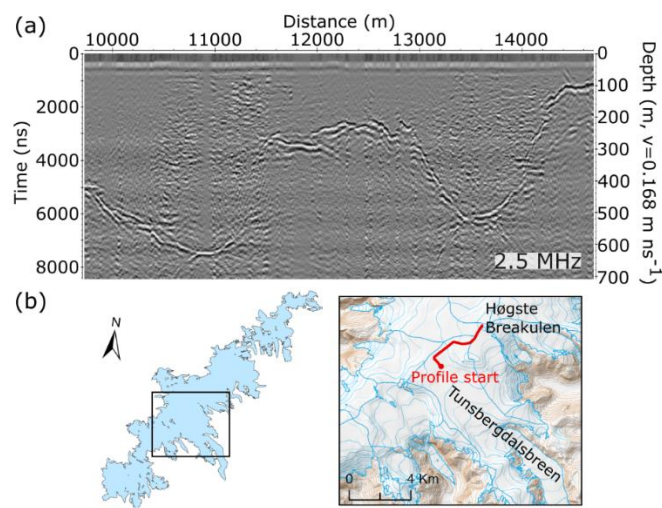


255 **Figure 3: Example of measurements with (a) 2.5 MHz, (b) 5 MHz and (c) 50 MHz antennas on shallow ice along a profile**  
travelling north near Grensevarden (Fig. 1). The 2.5 and 50 MHz profiles were collected along identical tracks in 2021,  
while the 5 MHz measurement are from 2022 along a profile located ~50 m from these tracks. The radargrams illustrate  
well the difference in resolution and penetration depth resulting from variations in antenna frequency. The lowest  
frequency measurements provide information on bed topography along the entire profile, while the 50 MHz profile  
allows for accurate measurements of thin ice and offers evidence of internal ice characteristics.

260



Following data processing, we observed a bed reflection along most 2.5 and 5 MHz radar segments and in higher frequency measurements collected in ice-marginal regions (Fig. 3). The bed reflections were delineated manually, and we calculated ice thickness from the reflection two-way travel time by assuming a constant radio-wave velocity in ice of  $0.168 \text{ m ns}^{-1}$ , similar to that used on other glaciers in Norway and abroad (Dowdeswell and Evans, 2004; Navarro and Eisen, 2009; Andreassen et al., 2012a; Yde et al., 2014; Johansson et al., 2022). The range of frequencies allows for a detailed mapping of both shallow and deep ice at the best possible resolution. In shallow regions, ice thickness was most accurately determined from the highest frequency measurements, which also provide information on snow (450 and 500 MHz data only), firn and internal layer characteristics (Fig. 3c). In this paper, we present only the interpreted ice thickness from these higher frequency measurements. In general, GPR measurements at Jostedalbreen are characterised by strong scattering and rapid attenuation of the radar signal (Fig. 3c), as is typical for radar surveys on temperate glaciers (Smith and Evans, 1972; Ogier et al., 2023). Occasionally, regions of more transparent ice were observed in the higher frequency measurements (Fig. 3c). These likely indicate either zones that are above the internal water table or isolated patches of cold (frozen) ice. While the 5 MHz antennas generally performed well in depths of up to 400–500 m, the advantage of using 2.5 MHz antennas was evident in areas with sloping bed topography (Fig. 3b) and in the deepest regions, where reflectors were sometimes weak or absent, even with the 2.5 MHz system (Fig. 4).

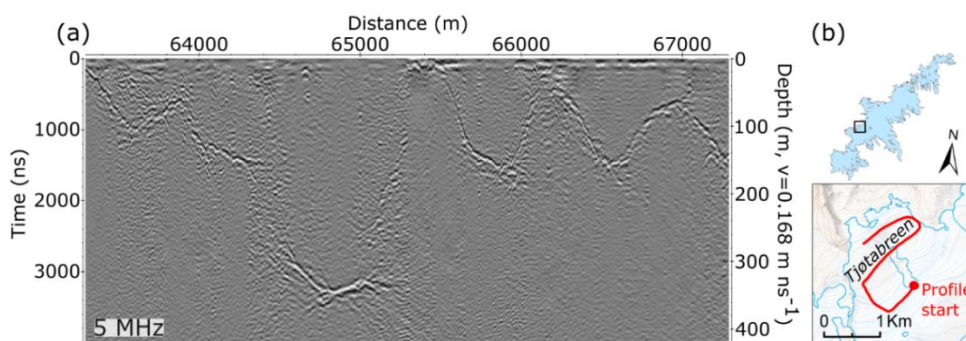


280 **Figure 4: (a) Example radargram of measurements with 2.5 MHz antennas. (b) The profile was located along a transect in the upper part of Tunsbergdalsbreen (Fig. 1), where the thickest ice was observed. The detailed background map in (b) is from the Norwegian Mapping Authority (WMS for Topografisk Norgeskart available at <https://www.geonorge.no/>) and the 2019 outline of glacier units on (b) is from Andreassen et al. (2022).**



285 The efficiency of snowmobile transport during the fieldwork depended strongly on the snow conditions and varied significantly between field seasons. For example, valley access onto Tunsbergdalsbreen was possible in 2022, when the snow cover was thick, but attempts to drive onto the glacier tongue in 2023 had to be abandoned. The helicopter measurements generally cover regions that were inaccessible on snowmobile, either due to steep and/or crevassed terrain, or unfavourable snow conditions. Consequently, helicopter measurements provide a valuable  
290 addition to the ground-based measurements. However, the airborne measurements generally had a lower penetration depth than ground-based measurements using the same antenna frequency, primarily due to increased electronic noise and radar wave attenuation, as well as scattering of the radar signal caused by large surface crevasses present in many airborne surveyed regions. Despite these challenges, bed reflectors were generally observed at depths of up to 350–400 m of ice in airborne measurements (Fig. 5).

295



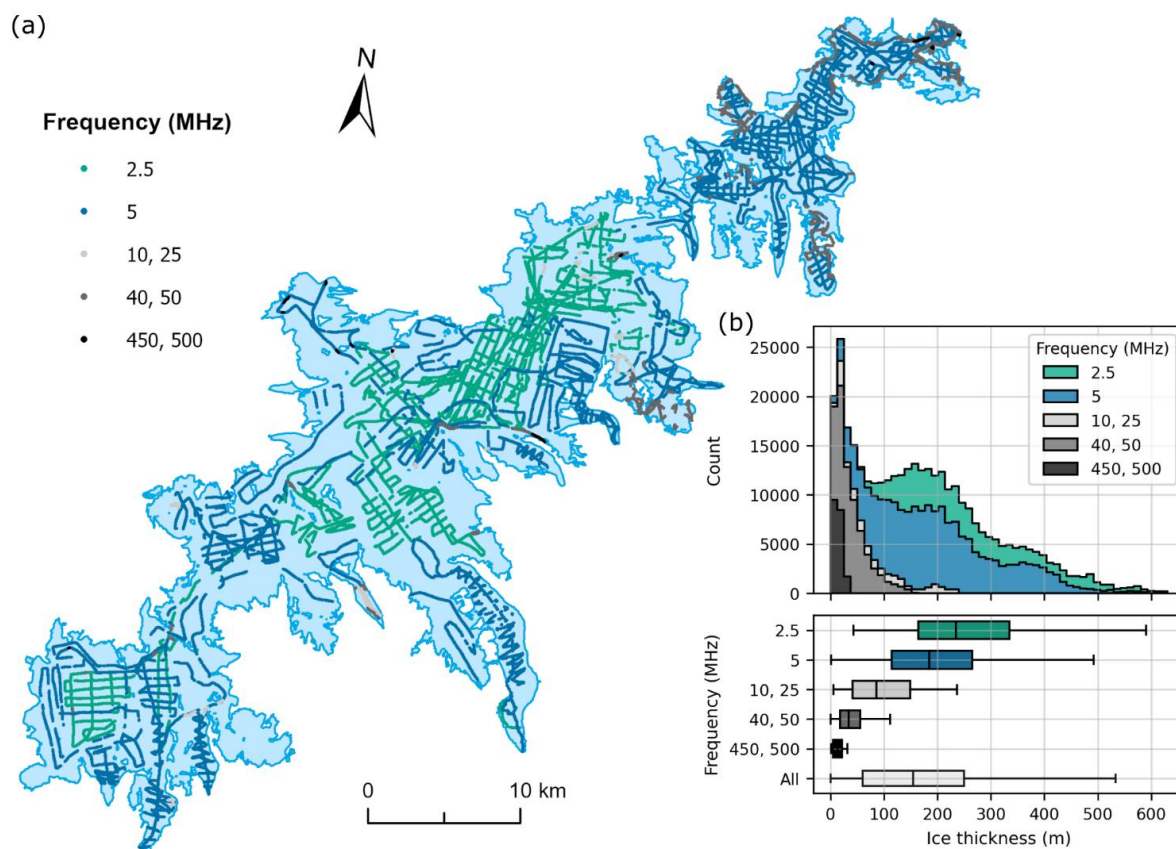
300 **Figure 5: (a) Example of measurements with the 5 MHz airborne radar system. (b) The profile was located along a transect at Tjøtabreen (Fig. 1). The background map in (b) is from the Norwegian Mapping Authority (WMS for Topografisk Norgeskart available at <https://www.geonorge.no/>) and the 2019 glacier outline is from Andreassen et al. (2022).**

After the initial ice thickness calculations, all observations of ice thickness were plotted in ArcGIS Pro, where we deleted points collected with the 5 and 2.5 MHz radar systems in sharp turns, as the long antennas were not fully  
305 extended in these locations. Profile lines collected alongside and in close proximity to valley walls were also removed to limit the influence of off-nadir reflections in the dataset. In marginal regions with both high- and ultra-high frequency observations, high-frequency measurements (2.5 and 5 MHz) were deleted due to their comparably lower accuracy. In order to produce a consistent dataset of ice thicknesses for the entire Jostedalbreen, we double-checked interpretations at all locations where ice thickness observations from crossing profiles differed by  
310 more than 15 m. When contrasting observations suggested that a transect was influenced by off-nadir reflectors or other uncertainties such as resolution issues, the presence of multiple reflectors or location uncertainties, these datapoints were removed from the dataset. The combination of multiple frequency measurements in many regions



of the ice cap has resulted in a dataset where both thin and very thick ice is represented in a generally satisfactory resolution (Fig. 6).

315



320

**Figure 6: (a) Ice thickness measurements across Jostedalsgreen categorized according to antenna frequency. The thickest regions of the ice cap were measured using the lowest frequency antennas, while higher frequencies were applied in the more marginal and thinner regions. (b) Histogram (top) and boxplot (bottom) of measurements of ice thickness categorised by antenna frequency. Boxes represent the interquartile range (IQR; the spread of the middle 50 % of the data), with medians indicated by vertical lines. Whiskers extend to the highest and lowest values that are within the 1.5\*IQR limits. The analysis shows that measurements collected using higher frequency GPR systems dominate at low ice thickness, while 5 and 2.5 MHz GPR systems were the better choice for ice thicknesses above ~100 m.**

### 325 3.3 Homogenization to 2020 DTM and calculation of glacier bed topography

Following the data processing and interpretation of the GPR measurements, the bed topography elevation beneath Jostedalsgreen was calculated from the point values of ice thickness and a recent 10 m national digital terrain model (DTM10) from the Norwegian Mapping Authority. For Jostedalsgreen, the DTM10 is derived from airborne laser scanning (lidar) collected by Terratec over a seven-day period in August 2020, that covered Jostedalsgreen



330 and surrounding area with a point density of minimum 2 pp m<sup>-2</sup> (Terratec, 2020). The central part of the ice cap  
was scanned on 9 August, the western part on 10 August and the eastern part on 15 August. The accuracy of the  
final point cloud is assumed to be ±0.1 m (Andreassen et al., 2023). The 2020 survey (2020 DTM) covers the entire  
Jostedalbreen, except for the lower tongue of Tunsbergdalsbreen (Andreassen et al., 2023) where surface  
elevation data in DTM10 is derived from stereophotogrammetry using 2017 orthophotos.

335

To prevent discontinuities in the elevation of bed topography, all ice thickness measurements were homogenised  
to correspond to the date of the 2020 DTM. We used DGNSS observations of surface elevation to calculate an  
area dependent mean surface elevation difference between the time of acquisition of GPR data and the 2020 DTM.  
Calculations show that DGNSS measurements exceed the DTM by average values ranging from 0.6 m (northern  
340 parts in spring 2022) to 3.9 m (central parts in spring 2018), reflecting surface changes such as the increased depth  
of the snowpack during spring measurements compared to the end of summer lidar scan. The elevation of the bed  
topography was calculated by subtracting the homogenised ice thicknesses from the 2020 DTM.

### 3.4 Ice thickness measurement uncertainties

The multifrequency dataset of crossing profiles allows for an investigation of discrepancies between measurements  
345 with various degrees of vertical resolution as a means to evaluate ice thickness uncertainties. Here, we present the  
results of a comparison of ice thicknesses at intersection points (crossover analysis), in addition to the total  
calculated measurement uncertainty for each datapoint following the method described by Lapazaran et al. (2016).  
In the final dataset, profiles crossed at 1207 locations (not counting profiles collected along identical tracks). Ice  
thicknesses in crossing points had a mean absolute difference (MD) of 6.8 m with a standard deviation (SD) of 5.8  
350 m, which when expressed in relation to ice thickness equals a MD of 5.0 % (7.1 % SD). Not surprisingly, the  
discrepancy between values increased with decreasing frequency and hence vertical and horizontal resolution.  
The largest discrepancies were observed where at least one of the crossing profiles was collected with 2.5 MHz  
antennas (MD of 8.4 m and a 6.7 m SD; maximum discrepancy of 39 m; n=538), whereas profiles collected with  
500 and 450 MHz antennas generally corresponded better with other observations (MD of 3.7 m and a 3.1 m SD;  
355 maximum discrepancy of 10 m; n=23). The crossover analysis also facilitated an assessment of the performance  
of the lowest frequency measurements when compared to higher resolution and more accurate ice thickness  
observations collected using antenna frequencies of 25–500 MHz. The comparison show that ice thicknesses  
measured with 2.5 and 5 MHz antennas were generally (but not always) somewhat larger than those measured  
with higher frequency antennas. The ice thicknesses measured with 2.5 and 5 MHz antennas were on average 8.0  
360 m (6.9 m SD; n=31) and 3.6 m (4.8 m SD; n=136) greater, respectively, than those measured with the 25–500 MHz  
antennas. It is unclear exactly why these differences occur. Although a systematic bias is unfortunate, the observed



differences are well below the vertical resolution (evaluated conservatively as  $\frac{1}{2}$  wavelength,  $\lambda$ ) of both the 2.5 MHz (33.6 m) and 5 MHz (16.8 m) antennas, as well as the total calculated measurement uncertainty described below.

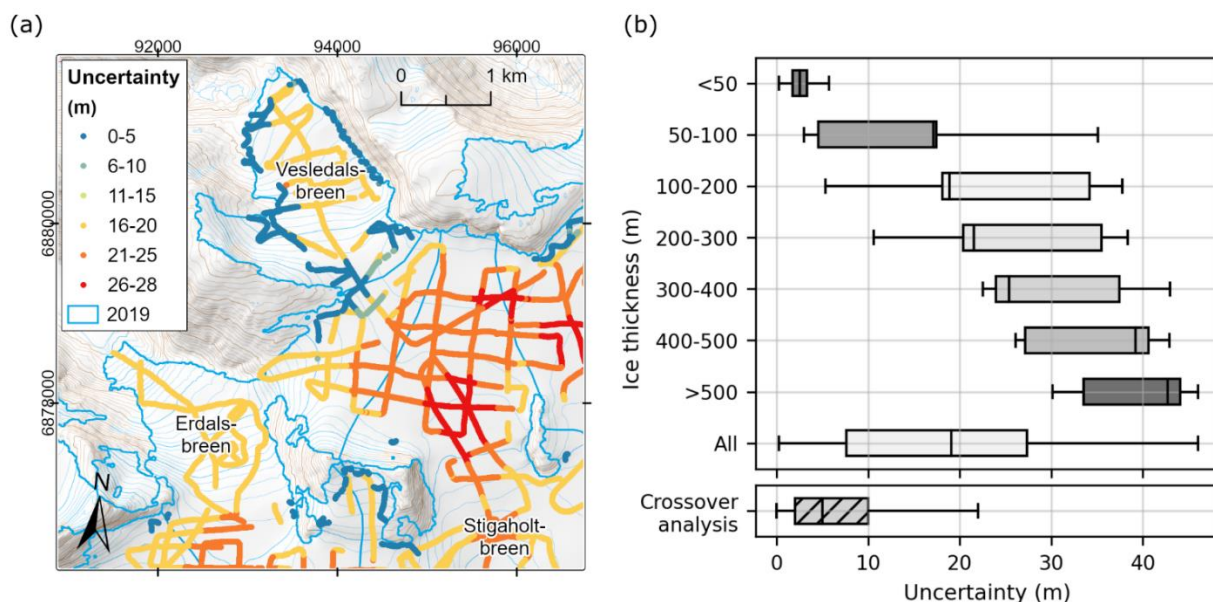
365 To evaluate the performance of the new 5 MHz helicopter system, we compared discrepancies between ice  
thicknesses measured at intersecting airborne and ground-based profiles. We found an MD of 7.2 m (4.6 m SD;  
n=56) between airborne and ground-based ice thickness measurements, which is comparable to values found for  
all ground-based and crossing 5 MHz profiles (MD of 6.5 m and a 5.0 m SD; n=705). It is worth noting that helicopter  
measurements along several outlet glaciers and at steep ice falls were conducted along centreline profiles, where  
370 off-nadir reflectors may affect the results (Fig. 1c). This could result in an underestimation of ice thickness in these  
regions. Where measurements along cross profiles suggested that the centreline values were unreliable, the latter  
were removed from the dataset. However, in most cases centreline values compared well with measurements  
along cross profiles and were largely included in the dataset.

375 As a crossover analysis does not encompass all potential uncertainties associated with ice thickness  
measurements, it is generally considered to only provide a rough approximation of uncertainty (Lapazaran et al.,  
2016). Consequently, we calculated the total measurement uncertainty for each ice thickness observation using  
the method described by Lapazaran et al. (2016), which is based on the root-sum-of-squares of both uncertainties  
in the ice thickness measurements and the measurement position. Using this approach, we included uncertainties  
380 related to the radio-wave velocity, which we assumed to be 5 %, as recommended by Lapazaran et al. (2016) when  
the same velocity is applied in both accumulation and ablation areas. In addition, our uncertainty calculations  
considered the signal resolution ( $\lambda/2$ ) and positioning uncertainty. The latter was accounted for by calculating the  
largest measured ice thickness difference within a circle, with the radius determined by the respective GNSS  
uncertainty. Using this approach, total ice thickness uncertainties were primarily controlled by antenna frequency  
385 and ice thickness because of their influences on vertical resolution and the uncertainty caused by the constant  
radio-wave velocity, respectively (Fig. 7 and Fig. B1).

The calculated combined uncertainties of the ice thickness measurements amounted to an average of 19.6 m for  
the entire dataset (SD of 12.1 m; n = 351 559), while mean ice thickness uncertainties ranged between 36.5 m (SD  
390 of 2.5 m) and 20.2 m (SD of 3.1 m) for 2.5 and 5 MHz measurements, respectively, and 1 m (SD of 0.5 m) for 450  
and 500 MHz measurements. The large mean uncertainty estimate calculated for most ice thickness observations  
was primarily a result of the conservative treatment of signal resolution and the assumed 5 % uncertainty from  
applying a single radio-wave velocity value to the entire ice cap despite ice cap-wide variations in snow, firn, and  
thermal ice conditions. The significantly larger measurement uncertainty found using the method of Lapazaran et  
395 al. (2016) compared to the crossover analysis (Fig. 7b), implies that the former approach leads to an overestimation



of uncertainties associated with relatively low frequency (below ~10 MHz) ice thickness measurements, particularly in regions with thick ice. We therefore suggest that the crossover analysis and the calculated measurement uncertainty represent a lower and upper estimate, respectively, of the uncertainties associated with each ice thickness observation. In the datafile compilation presented here, we include only the upper estimate of total measurement uncertainty.



405 **Figure 7: (a) Calculated ice thickness measurement uncertainties at Vesledalsbreen (Fig. 1). Variations in measurement uncertainties are primarily controlled by antenna frequency, with <5 m uncertainty for 500 MHz measurements, between 6 and 13 m uncertainty for 50 MHz measurements and  $\geq 14$  m for 5 MHz measurements. The largest measurement uncertainties are found in regions with thick ice, illustrating the influence of ice thickness on the uncertainty calculations. (b) Distribution of calculated absolute uncertainty in ice thickness by thickness class and for all measurements following the method described by Lapazaran et al. (2016), as well as that observed in the crossover analysis. Boxes represent the interquartile range (IQR; the spread of the middle 50 % of the data), with medians indicated by vertical lines. Whiskers extend to the highest and lowest values that are within the 1.5\*IQR limits. The background map in (a) is from the Norwegian Mapping Authority (WMS for Topografisk Norgeskart available at <https://www.geonorge.no/>) and the 2019 outline of Jostedalsglacier units is from Andreassen et al. (2022). The coordinate system is UTM 33N, datum ETRS\_1989.**

### 3.5 Description of datafile compilation

415 The ice thickness point values from Jostedalsglacier were compiled in a format similar to that of the Glacier Thickness Database (GlaThiDa Consortium, 2020; Welty et al., 2020) for straight-forward application in future studies. Data were stored in a CSV (comma-separated values) file with attributes describing the data (Table 2), and a DOI is provided for the ice thickness dataset. Consequently, the dataset follows the FAIR principles of optimised findability, accessibility, interoperability, and reusability.





420

**Table 2: Attributes used in the point dataset of ice thickness values on Jostedalsgreen.**

Attributed field	Unit	Description
SURVEY_DATE	YYYYMMDD	Survey date
PROFILE_ID	Text	Identifier of processed radar profile
POINT_ID	Number: 1-n	Point identifier
ANTENNA_FREQUENCY	MHz	Antenna frequency of measurement
SURVEY_METHOD	Text: H, S or F	Means of transport during survey (H: Helicopter, S: Scooter, F: Foot)
GNSS_SOURCE	Number: 0 or 1	Position information (0: Radar GNSS (lowest uncertainty) and 1: External GNSS source or some degree of interpolation across minor data gaps)
POINT_LAT	DDD.DDDDDD°	Latitude of point value
POINT_LON	DDD.DDDDDD°	Longitude of point values
GNSS_ELEVATION	m a.s.l.	Surface elevation from GPR GNSS
THICKNESS	Meter	Ice thickness value
THICKNESS_UNCERTAINTY	Meter	Uncertainty in ice thickness based on Lapazaran et al. (2016)
THICKNESS_2020DTM	Meter	Ice thickness value homogenised to the 2020 DTM surface. Corrected for differences in surface elevation during survey years relative to the 2020 DTM.

\*Survey date August 2020 except for the lower part of Tunsbergdalsgreen.

Most of the attributes in the table containing ice thickness point values are self-explanatory and identical to those in GlaThiDa. However, data entries such as SURVEY\_METHOD, GNSS\_SOURCE and THICKNESS\_2020DTM are additional attributes to describe the Jostedalsgreen data collection. In addition to the datafile containing the complete ice thickness dataset ( $n = 351\,559$  entries), we provide a thinned-out version of this dataset ( $n = 35\,100$  entries) consisting of point values extracted randomly from the full dataset but with a minimum distance of 20 m. The smaller dataset allows for easier plotting and analysis.

### 3.6 Model-based ice thickness extrapolation

While the dense network of GPR profiles across large parts of the ice cap provides direct local information on ice thickness on 59 out of the 81 glacier units that make up Jostedalsgreen ice cap (Fig. 1), an extrapolation to unmeasured regions was necessary to produce grids of ice thickness and bed topography which cover the entire Jostedalsgreen. Here, we apply an approach that combines the advantages of inter- and extrapolation of ice thickness observations with those of ice thickness modelling from an inversion of surface topography (Huss and



Farinotti, 2014; Grab et al., 2021). The basis of this approach is an ice thickness model originally developed for global-scale applications (Huss and Farinotti, 2012). The model was used in the Ice Thickness Model Intercomparison eXperiment (ITMIX and ITMIX2, Farinotti et al., 2017, 2021) and performed well in estimations of ice thickness distribution and bed topography. The general concept of the model is to derive local ice thickness  
440 from surface characteristics. It relies on glacier surface hypsometry of all individual glacier units of Jostedalsbreen, discretised into 10 m elevation bands. Variations in the valley shape and the basal shear stress along each outlet glacier's longitudinal profile, as well as an estimated longitudinal trend in basal sliding (e.g., Huss and Farinotti, 2012), are taken into account. Ice volume fluxes are computed along a longitudinal profile based on calibrated mass balance gradients. Subsequently, ice thickness is calculated by inverting the flow law for ice (Glen, 1955).  
445 Resulting averages of elevation-band ice thickness are then extrapolated to a regular grid by considering both local surface slope and distance from the glacier margin, excluding ice divides (for details see Huss and Farinotti, 2012).

Before initialising the model-based ice thickness extrapolation, we harmonised the spacing of the acquired profiles by taking the average of all homogenised ice thickness point data contained within the same 10 x 10 m cell of the  
450 DTM10. The ice thickness point dataset and the outline of Jostedalsbreen both serve as important input when computing spatially distributed ice thickness. As glacier outline, we used the national glacier inventory which relies on Sentinel-2 images taken on 27 August 2019 (Andreassen et al., 2022). In this dataset, Jostedalsbreen is divided into glacier units from topographic observations on ice divides. The inventory was derived using a standard semi-automatic method and checked against orthophotos and Sentinel composites from 2017 and 2019, respectively,  
455 with manual edits to correct for areas in shadow, with debris-cover, and lake outlines. The uncertainty in the outlines of the final product was estimated to be within half a pixel ( $\pm 5$  m).

Our dataset of distributed ice thickness for all Jostedalsbreen was produced by optimising modelled ice thickness to local ice thickness observations for each individual glacier unit, following a three-step procedure that consisted  
460 of (i) model optimisation, (ii) spatial bias-correction of modelled thicknesses, and (iii) spatial interpolation relying on point values of thickness and bias-corrected model results for regions that are not covered by GPR surveys.

In step (i), we optimised the apparent mass-balance gradient (Farinotti et al., 2009) in an automatic procedure to minimise the average misfit between modelled ice thickness and the available observations for each of the 59 outlet  
465 glaciers with ice thickness measurements. The apparent mass balance was then computed based on two linear elevation gradients, one for the ablation area and one for the accumulation area, assuming a balanced mass budget for the entire glacier unit. The resulting apparent mass balance distribution was then used to compute ice volume fluxes from the top to the bottom of each glacier unit, and to infer modelled ice thickness distribution as in Andreassen et al. (2015).



470

In step (ii), the modelled ice thickness distribution from step (i) was bias-corrected using ice thickness point values. First, relative differences between modelled and measured point ice thickness distributions were evaluated. These differences were then spatially inter- and extrapolated based on an inverse-distance weighting scheme. This relative spatial ice thickness correction field was then superimposed on the modelled ice thickness distribution, resulting in a bias-corrected model-based ice thickness distribution that accounts for the differences between observed and modelled ice thickness at a spatially distributed scale. Nevertheless, this ice thickness distribution will not exactly match all GPR-derived point values of thickness.

In the final step (iii), we spatially interpolated the ice thickness distribution based on (1) all available ice thickness observations, (2) the model results adjusted in steps (i) and (ii) in regions that were not covered by direct measurements (buffered in a distance of 100–200 m around available observations depending on outlet glacier size), and (3) the condition of zero ice thickness on the glacier margin, except for ice divides. The ice thickness at ice divides was obtained from model results of neighbouring outlet glaciers, and also entered the interpolation. Furthermore, a set of individually estimated thicknesses on ice divides based on local knowledge and direct interpolation of nearby GPR profiles was included to increase the robustness of spatially complete ice thickness estimates at ice divides. Repeating the complete procedure several times ensured convergence and thus consistency of thicknesses on both sides of the ice divides. For glacier units without GPR measurements, the ice thickness model was run using average calibrated parameters of the apparent mass-balance gradient from all outlet glaciers with direct observations. This direct modelling of ice thickness, however, was only relevant for small and mostly thin glacier units within Jostedalsgreen, and account for just 1.9 % of the total inferred volume of the ice cap. We finally combined all results of extrapolated ice thickness from the 81 glacier units contained in Jostedalsgreen into a complete coverage with a spatial resolution of 10 x 10 m.

### 3.7 Bed topography and potential future lakes

Bed topography was obtained by subtracting distributed ice thickness from the DTM10 ice surface elevation. The resulting grid of bed topography was then smoothed with a spatial filter of 50–100 m (depending on glacier basin area) to remove remaining discontinuities at ice divides, as well as unrealistic small-scale variability in calculated bed topography that cannot be inferred with the applied methodology and will originate from surface features. Depressions in the bed topography might act as potential future lakes after complete disappearance of the ice cover. Even though the uncertainty in detecting the extent and volume of such depressions is large, we derived a map of potential lake area and depth from the map of subglacial bed topography. This was achieved by using a sink fill algorithm that detected depressions, after which the depth and volume of each depression was determined



by artificially filling the depression until they overflow. This resulted in an inventory of individual potential glacier lakes, including the relevant attributes, such as their elevation, area, volume, or maximum depth.

### 3.8 Uncertainties in extrapolated ice thickness

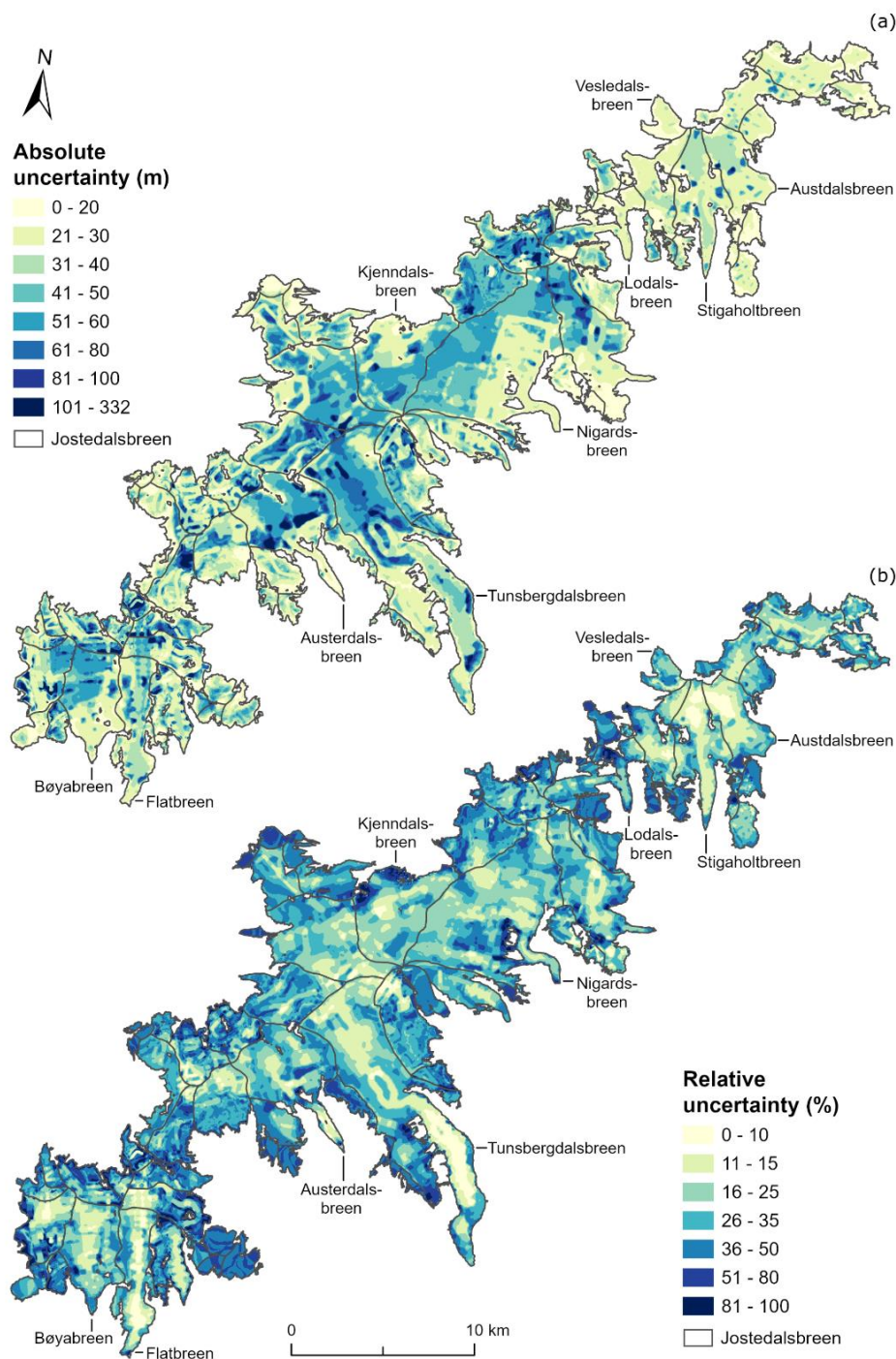
505 The uncertainty in extrapolated ice thickness is composed of two elements: (1) the uncertainty in measured ice thickness, and (2) the uncertainty induced when extrapolating point ice thickness across the entire ice cap supported by the model-based approach. These two elements of uncertainty are estimated separately, and then propagated through the methodology described above to derive a spatially distributed uncertainty map for the entire ice cap. As described in section 3.4, the uncertainty associated with each point value of ice thickness was calculated  
510 following Laparazan et al. (2016). We conservatively assume all uncertainties across the entire ice cap to be correlated and generate a dataset with maximum observed thickness and minimum ice thickness according to the above uncertainties. Based on these two datasets, we repeated the approach described in section 3.6 using each of these datasets. Taking the mean local deviation of the results from the ice thickness distribution inferred with the reference approach, we computed a spatially distributed uncertainty estimate due to measurement uncertainty.

515

To assess the uncertainty caused by extrapolating observations to unmeasured regions, we performed a suite of sensitivity experiments by varying different parameters of the model-based approach within conservatively set, but physically meaningful, ranges. This was performed for the viscosity of ice, the assumed fraction of basal sliding, and the apparent mass balance gradients. In each experiment, the reference dataset of point ice thickness values  
520 was used for calibration, such that the resulting ice thickness grids differ mostly in regions where ice thickness is solely inferred by the model.

Finally, we combined the local offset from the reference ice thickness distribution for all experiments based on the root-sum-of-squares resulting in an absolute and a relative uncertainty grid (Fig. 8). Local uncertainties were  
525 bounded to not exceed the grid cell's reference ice thickness which occurred in a few instances close to glacier margins. Typically, this grid indicates small uncertainties close to the GPR profiles and larger uncertainties in regions where the result is based on ice thickness modelling. Overall, we find a mean uncertainty in local ice thickness of 36 m (30 %), where regions with thick ice are characterised by high absolute but low relative thickness uncertainties, and vice versa for regions with thin ice (Fig. 8).

530



535 **Figure 8: (a) Absolute and (b) relative uncertainty for distributed ice thickness on Jostedalsbreen. The two figures illustrate that the largest absolute uncertainties appear in regions with thick ice and away from GPR profiles, while the largest relative uncertainties are found in the thin ice marginal regions. The 2019 outline of Jostedalsbreen glacier units is from Andreassen et al. (2022).**

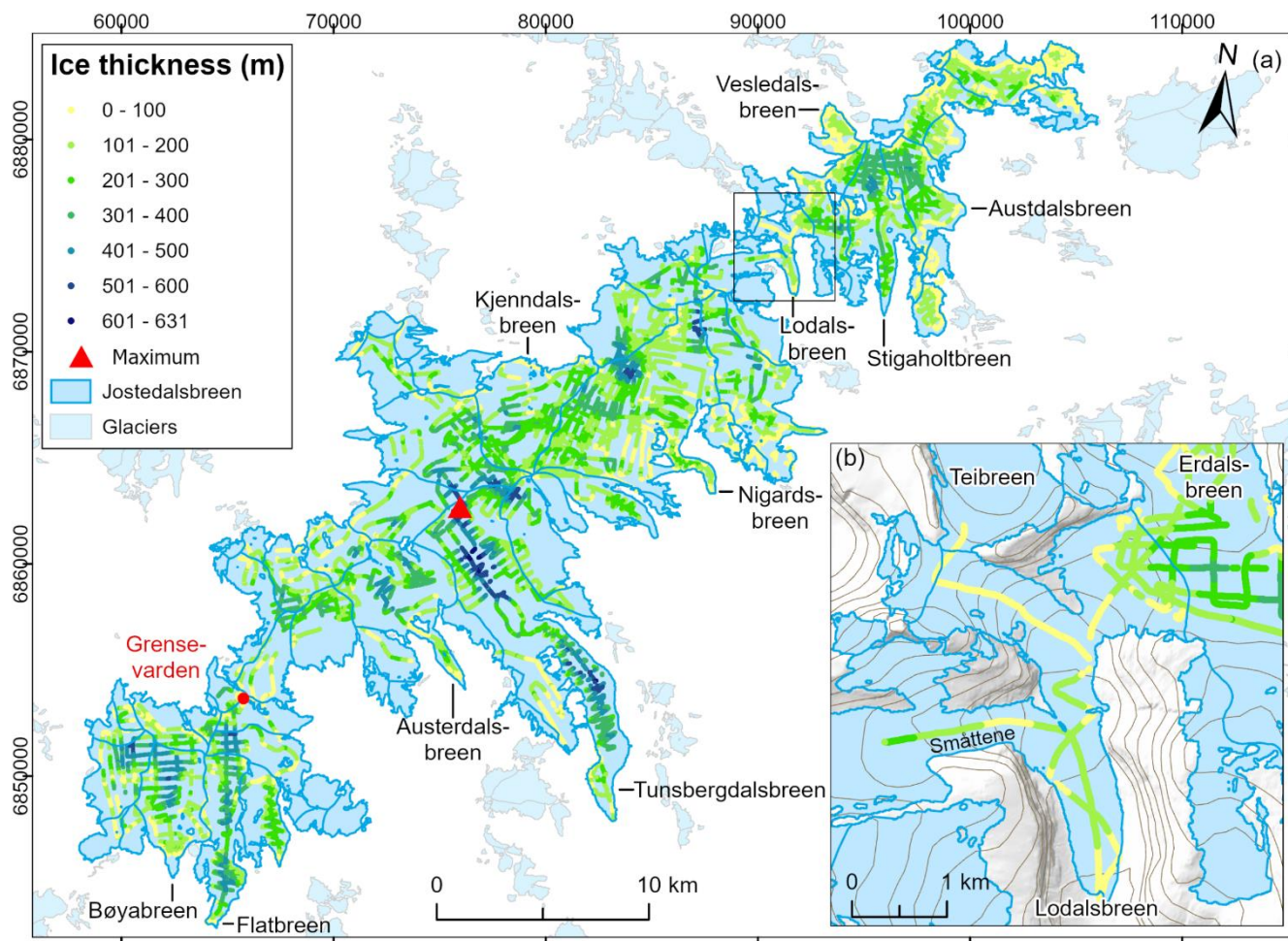


## 4 Results

### 4.1 Measurements of ice thickness

The dataset presented here provides ice thickness point values for 59 of the 81 glacier units that constitute the Jostedalsgreen 2019 inventory. These 59 glaciers cover 437 km<sup>2</sup>, or 95 % of the total area of the ice cap (458 km<sup>2</sup> in 2019). All parts of Jostedalsgreen are now less than 900 m from a point of known ice thickness (measurement or glacier outline), while distances to a known point are less than 300 m for 90 % of the ice cap and less than 100 m for 49 % of the ice cap. A maximum ice thickness of 631 m (or 628 m when referring to 2020 DTM) was measured in the upper accumulation area of Tunsbergdalsgreen, which is the largest outlet glacier of Jostedalsgreen and located in the central part of the ice cap (Fig. 4 and 9). In Jostedalsgreen South and North, ice thickness reaches maximum values of ~520 and ~430 m, respectively. In general, the thickest ice at Jostedalsgreen is found in the flattest areas of the ice cap, while thinner ice of less than 100 m thickness covers protruding hills. In the northern parts, the highest mountains in the landscape surrounding Stigaholtgreen (Fig. 7 and 9) are already partially ice-free, giving the ice cap a more disjointed appearance in this region.

Along the south-eastern margin of Jostedalsgreen, large outlet glaciers flow far into the valleys below. Particularly thick ice is found along the three glacier tongues of Tunsbergdalsgreen (up to ~615 m), Flatgreen (up to ~435 m) and Stigaholtgreen (up to ~320 m) (Fig. 9). These outlet glaciers are characterised by large accumulation areas from which ice flows relatively unrestricted from the innermost parts of the ice cap plateau and along deep glacier-carved valleys. In comparison, thinner ice is observed along outlet glaciers where ice flows from the ice cap plateau through steep ice falls. Austerdalsgreen with its two steep ice falls and low-sloping glacier tongue, represents one such example. Here, helicopter measurements along the centre flowline of the largest of the two narrow ice falls suggest that the ice is only 40–50 m thick in the steepest parts. Below the ice falls, ice thickness reaches a maximum of ~235 m. At Nigardsgreen, ice also thins to 40–50 m as it flows through the two smallest western ice falls. Here, the main flow of ice from the ice cap plateau appears to occur through the much larger northern tributary, where centre-line ice thicknesses of more than 100 m were measured in the thinnest regions. Below the three ice falls, ice thickness reaches a maximum of ~265 m before thinning towards the famous glacier front of Nigardsgreen.



565 **Figure 9: (a) Combined ice thickness observations from the field campaigns in 2018, 2021, 2022 and 2023. The point of**  
**maximum thickness is marked with a red triangle. (b) Section of Lodalsbreen with 100 m surface contours. Note that**  
**the helicopter measurements along Lodalsbreen were collected during the first test flight of the airborne radar system,**  
**where profile locations were positioned less than ideal in relation to the valley orientation. The background mountain**  
570 **shadow and 100 m contour lines in (b) are from the Norwegian Mapping Authority (WMS for Topografisk Norgeskart**  
**available at <https://www.geonorge.no/>). The 2019 outline of Jostedalsglacier units is from Andreassen et al.**  
**(2022) and the coordinate system is UTM 33N, datum ETRS\_1989.**

575 From the extensive measurements of ice thickness, we have identified two regions that may be particularly  
vulnerable to future climate-forced changes and that have the potential to separate Jostedalsglacier into three  
unconnected ice caps, North, Central, and South (Fig. 1). In the north, Lodalsbreen currently connects the  
northernmost part of Jostedalsglacier with its more southern regions through three steep tributaries (Fig. 9b).  
Helicopter measurements along the centre flowlines reveal that the ice thins to 50 m or less as it flows southwards  
and into the incised valley below. Ice flowing from the western tributary is thicker, with ice thicknesses ranging  
580 between 50 and 70 m along its thinnest sections. Further south on Jostedalsglacier, thin ice of less than 25 m covers



the narrow stretch at Grensevar den that joins the southern part of the ice cap with its central regions (Figs. 3 and 9). Bedrock has already started protruding through the thinning ice, and the emerging rocks are likely to further accelerate the changes occurring in this part of Jostedalsbreen due to positive feedback on melting from a decreasing albedo of the surroundings. However, it is important to note that while thin ice may indicate increased vulnerability to future warming, other factors such as ice velocity and surface mass balance are important influences when considering future changes in areas with thin ice. Such considerations require ice cap-wide modelling of glacier evolution and are beyond the scope of this paper.

#### 4.2 Comparison to previous ice thickness measurements at Jostedalsbreen

The new comprehensive dataset of Jostedalsbreen ice thicknesses represents a significant improvement to previous measurements, both in relation to data quality and spatial coverage across the ice cap. We now have a much better understanding of ice thickness variations in the region and have also extended the maximum measured ice thickness from 600 m measured during the 1980s field campaigns (Sætrang and Wold, 1986) to the 631 m measured in 2021. Many of the previous ice thickness measurements conducted on Jostedalsbreen have considerable uncertainties in measurement positioning and surface topography. Therefore, we limit the comparison of our measurements to ice thickness observations on Austdalsbreen in the late 1980s, which we consider to be afflicted with the lowest uncertainties. This older dataset was collected to evaluate future changes to Austdalsbreen due to enhanced calving after the regulation of the proglacial lakes Austdalsvatnet and Styggevatnet for hydropower production (Hooke et al., 1989; Laumann and Wold, 1992). Ice thickness was measured in nine hot water drilled boreholes and by GPR within an area of 600 by 1000 m, where the ice thicknesses ranged between 100 and 230 m (Sætrang and Holmqvist, 1987; Sætrang, 1988). The boreholes were drilled in September 1986 and October 1987, while the GPR measurements used here for the assessment of uncertainties were collected in April–May 1988 using an 8 MHz radar system. Comparisons between radar measurements and boreholes at the time showed borehole bedrock elevations between 14 m below and 1 m above radar bed elevations. The overall uncertainty of the radar bed elevations was estimated to be within 7 m based on results from a radar crossover analysis and observed uncertainties in positioning and surface elevation (Sætrang, 1988).

Two radar profiles from 2022 intersected the area also mapped by GPR in 1988. To allow for a comparison with the new ice thickness measurements, we interpolated a 5 x 5 m bed elevation grid from the 1988 GPR measurements and extracted the bed elevations at the nine boreholes and 454 locations covered by the GPR survey in 2022. On average, bed elevations measured in boreholes were 4 m lower than the interpolated grid, and the grid consequently shows a good replication of variations observed in both of the two older datasets. When comparing values from the interpolated grid and those obtained in 2022, we find that bed elevations calculated





615 from measurements in 2022 were on average 14 m lower than those found with GPR in 1988 (i.e., 2022 ice was thicker than expected from the 1988 dataset). However, it is unclear whether this discrepancy relates to uncertainties concerning the earlier or the new measurements. In this region the 2022 measurements have a measurement uncertainty of 17–20 m (Fig. B1), and the observed discrepancies are consequently within the range of combined uncertainties.

### 4.3 Distributed ice thickness, bed topography and potential future lakes

620 The maps of ice thickness and bed topography (Fig. 10) allow for a coherent description of the variations in the morphology of Jostedalsgreen, also in regions that are not covered by GPR measurements. The two grids illustrate that thickest ice is found predominantly away from ice divides and in the prominent subglacial valleys of the largest outlet glaciers. By contrast, thinner ice and elevated subglacial bed topography are often associated with regions of the ice cap with high surface elevations. From the modelled ice thickness grid, we calculate an ice cap-wide mean ice thickness of 154 m  $\pm$ 22 m and a present (~2020) ice volume of 70.6  $\pm$ 10.2 km<sup>3</sup> (Table 3). Overall, the presented results are consistent with previous estimates for Jostedalsgreen, and any smaller discrepancies are well within the uncertainty of the applied methodologies. The calculated mean ice thickness is slightly smaller than the earlier estimate of 158 m which was calculated for an interpolated region covering 65 % (310 km<sup>2</sup>) of the 2006 area (474 km<sup>2</sup>) of Jostedalsgreen (Andreassen et al., 2015). Our calculated ice volume also compares well with the estimate of 72.6 km<sup>3</sup> provided by Frank and van Pelt (2024).

630

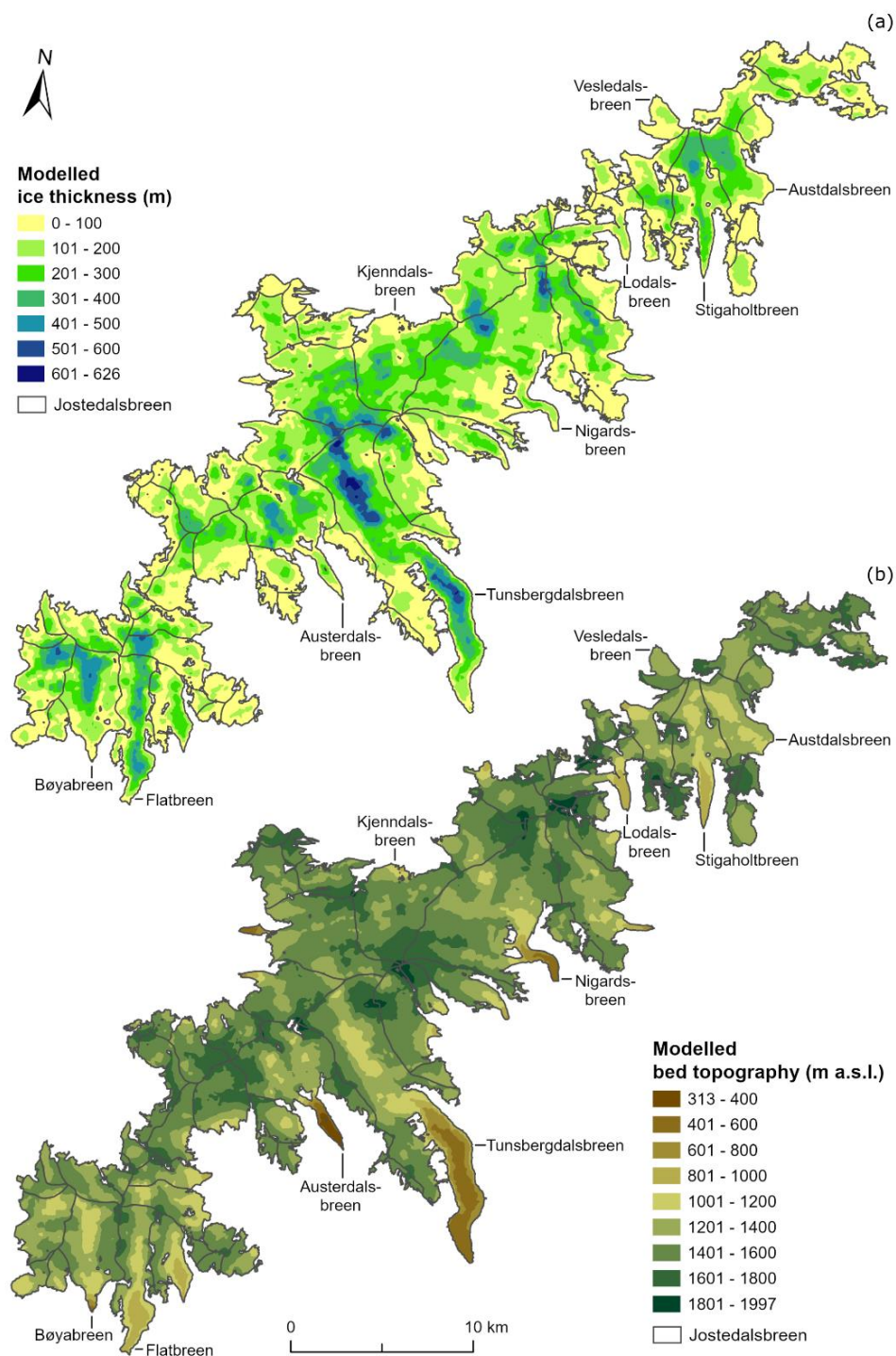


**Figure 10: (a) Modelled distributed 10 m ice thickness of Jostedalsbreen and (b) distributed 10 m bed calculated from DTM10 and the modelled ice thickness distribution (Fig. 10a). The 2019 outline of Jostedalsbreen glacier units is from Andreassen et al. (2022).**



635

Calculations of key numbers for selected elements of the ice cap (Table 3) show that Jostedalsbreen Central is by far the largest of the three regions when comparing area, mean ice thickness and volume. The two surrounding regions have much smaller areas and ice is generally thinner, in particularly in the smallest northernmost region.

640 The ice thickness measurements presented in section 4.1 illustrate the vulnerability of Jostedalsbreen to future separation into three minor ice caps. Following a future breakup, Jostedalsbreen Central would remain the largest glacier in Norway and mainland Europe, surpassing the second largest glacier, Vestre Svartisen, which had an area of 192.2 km<sup>2</sup> in 2019 (Andreassen et al., 2022).

645 **Table 3: Key numbers for the three regions and prominent outlet glaciers based on calculations from the model-based grid of ice thickness for Jostedalsbreen. The bracketed values after each glacier name refer to glacier IDs from Andreassen and Winsvold (2012b). Data coverage is defined as all regions which are less than 300 m from a point of known ice thickness (measurements or glacier outline), with bracketed values specifying the percentage of the area which are less than 100 m from a known point.**

Glacier	Area (km <sup>2</sup> )	Maximum (m)	Mean (m)	Volume (km <sup>3</sup> )	Data coverage (%)
Jostedalsbreen	458.1	626	154	70.6	90 (49)
North	69.3	432	123	8.5	99 (69)
Central	309.6	626	161	49.9	88 (45)
South	79.3	518	155	12.3	91 (47)
Lodalsbreen (2266)	8.8	329	93	0.88	98 (57)
Kjenndalsbreen (2296)	19.1	419	186	3.6	92 (50)
Nigardsbreen (2297)	41.7	572	178	7.4	98 (62)
Nigardsbreen MB* (2311, 2299 and 2297)	45.4	572	169	7.6	98 (62)
Tunsbergdalsbreen (2320)	46.2	626	233	10.8	89 (45)
Austerdalsbreen (2327)	19.4	510	191	3.7	85 (44)
Bøyabreen (2349)	13.8	501	201	2.8	99 (53)
Flatbreen/Supphellebreen (2352)	12.7	452	205	2.68	97 (58)
Austdalsbreen (2478)	10.3	402	188	1.98	100 (70)
Stigaholtbreen (2480)	12.5	432	188	2.38	99 (65)

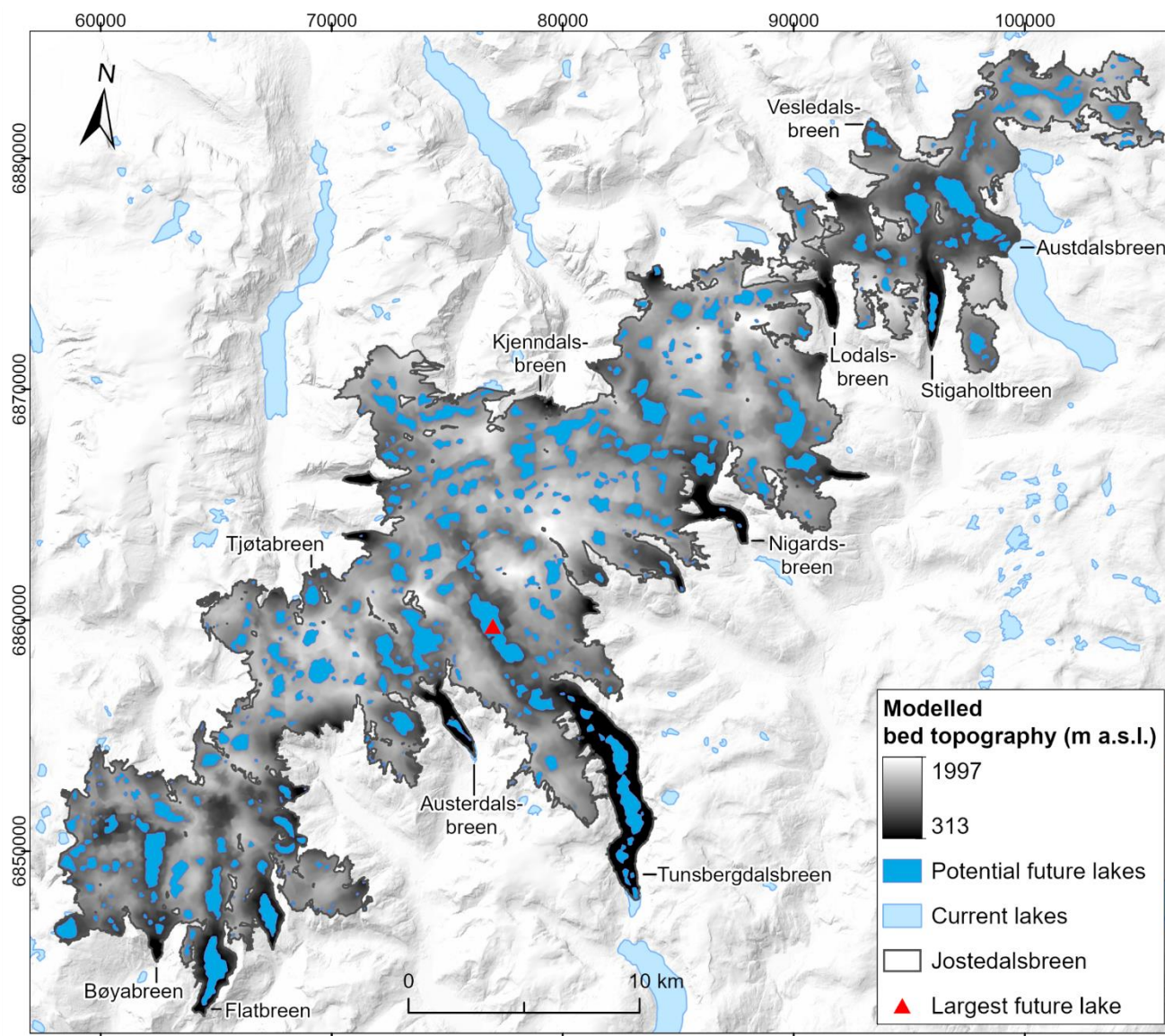
650 \*Nigardsbreen MB refers to the mass balance glacier basin used by Andreassen et al. (2023).

Beneath Jostedalsbreen we observe a versatile landscape of deep glacially incised valleys that extend to the centre of the ice cap in some regions, and are surrounded by steep valley walls, hanging valleys and glacial over-



655 deepenings (Fig. 10b). The map of bed topography provides a glimpse of how the landscape would look like if  
Jostedalsbreen was to completely disappear and from it we can infer possible future changes in the regional  
hydrological systems. While a detailed analysis of hydrological changes in the region is outside the scope of this  
study, it is worth noting that several glaciers have discrepancies between the ice divides defined by the current  
surface topography of the ice cap and the hydrological catchment boundaries determined by the bed topography  
in an ice-free landscape. Examples of such are Flatbreen (Supphellebreen), Tunsbergdalsbreen and  
660 Nigardsbreen, where the subglacial valleys appear to extend significantly beyond the current ice divides (Fig. 10b).  
Other glaciers, such as at Austerdalsbreen and Lodalsbreen, have similar surface and subglacial topographical  
divides. Overall, it appears likely that in an ice-free landscape, upper catchment boundaries in the central and  
southern Jostedalsbreen regions will, in many places, be located further north and northwest than the currently  
more central longitudinal ice divide. In the northern parts of Jostedalsbreen, the potential extent of ice-free  
665 catchment areas appears more uncertain due to several smaller thresholds in the bed topography and limitations  
in data coverage across these. Consequently, we tentatively suggest that in an ice-free landscape, the topographic  
bed catchment at Austdalsbreen may increase substantially in size at the expense of the surrounding regions,  
although further analysis is required to substantiate this claim.

670 The distributed bed topography furthermore reveals subglacial bed depressions as likely locations for future lakes  
in a warming climate (Fig. 11). Our results show a multitude of potential lakes, the largest of which is 3.5 km long  
and has an area of 2.4 km<sup>2</sup> and is located in the inner regions of Tunsbergdalsbreen, just south of where the  
thickest ice was measured. Other large topographic depressions are found north of Bøyabreen and Flatbreen  
glacier fronts, underneath the glacier tongue of Tunsbergdalsbreen, and north-west of the calving front of  
675 Austdalsbreen. According to our estimates, a total of 14 % (65.3 km<sup>2</sup>) of the present-day glacier area of 458 km<sup>2</sup>  
(2019) can be covered by lakes if the entire Jostedalsbreen melts away.



680 **Figure 11: Location of current and potential future lakes calculated from the grid of subglacial bed topography at Jostedalsglacier (Fig. 10b). The largest potential future lake is marked by a red triangle. The 2019 outline of Jostedalsglacier is from Andreassen et al. (2022) and the background mountain shadow and outline is from the Norwegian Mapping Authority. Outline of present-day lakes is from the Norwegian Mapping Authority (WMS for Topografisk Norgeskart available at <https://www.geonorge.no/>) and the Norwegian Water Resources and Energy Directorate (<https://doi.org/10.1017/jog.2022.20>). The coordinate system is UTM 33N, datum ETRS\_1989.**

685



## 5 Data availability

All ice thickness observations (complete and thinned-out compilations) and maps of ice cap-wide ice thickness, combined uncertainty in ice thickness, bed topography and outlines of potential future lakes are available for download at <https://doi.org/10.58059/yhwr-rx55> which is hosted by the Norwegian Nasjonalt Vitenarkiv (Gillespie et al., 2024).

## 6 Conclusions

In this paper we present a rich point dataset of high-quality ice thickness observations on Jostedalbreen ice cap collected during GPR surveys in 2018–2023. Measurements were collected from 59 of the 81 glacier units that constitute Jostedalbreen and 90 % of the total ice cap area is now less than 300 m from a point of known ice thickness. A maximum ice thickness of ~630 m was measured on Tunsbergdalsbreen outlet glacier in the central part of the ice cap. This measurement exceeds the 600 m maximum thickness previously measured on Jostedalbreen (Sætrang and Wold, 1986; Andreassen et al., 2015). Smaller maximum ice thicknesses of ~520 m and ~430 m were measured in the southern and northern parts of the ice cap, respectively. Using this new dataset of ice thickness values, we produce model-based grids of distributed ice thickness and bed topography that allow for a coherent description of ice thickness variations and subglacial morphology over the entire Jostedalbreen, as well as calculations of key figures for the ice cap. We find that Jostedalbreen has a mean thickness of 154 m  $\pm$  22 m and a present (~2020) ice volume of 70.6  $\pm$  10.2 km<sup>3</sup>. Together, the ice thickness measurements and distributed datasets provide exceptional new details about the geometry and bed topography of Jostedalbreen, revealing vulnerabilities to future ice cap fragmentation and possible changes in the hydrological systems with climate warming. These datasets will form the basis of future studies of climate-induced changes in the Jostedalbreen region, which are of high importance to local stakeholders such as farmers, tourist operators and hydropower companies.

## Author contributions

MKG, JCY, and LMA designed the study. MKG led the data collection of ice thickness measurements and MKG, SDV, KHS, JA, JB, JMC, HE, BK, EL, MM, KM, SDN, TOR, EWNS and KØ carried out the fieldwork. MKG subsequently processed and interpreted the ice thickness data. MH ran the model-based extrapolation of ice thickness measurements and prepared all distributed datasets while MKG, LMA and KHS produced the figures. MKG, LMA and MH prepared the manuscript with contributions from all co-authors. JCY was the principal investigator of the JOSTICE project.

715



## Acknowledgements

We would like to express our sincere gratitude to all who have contributed to the planning and implementation of the comprehensive and challenging fieldwork that was required to adequately map ice thickness across Jostedalsbreen. Especially, we would like to thank Ingebjørg Haugland for assisting during the 2021 field campaign  
720 and Jostedalsbreen National Park, Nigardsbreen Nature Reserve, Breheimen National Park and the municipalities of Luster, Stryn, Sogndal, Sunnfjord and Skjåk who all granted permissions for the fieldwork. We would also like to thank Airlift AS who provided logistical support during both ground-based and airborne radar surveys. Steinmannen and Statkraft-hytta mountain huts, both owned by Statkraft, generously accommodated us during the fieldwork and snowmobiles were provided by Vang Auto-Service AS, Luster Red Cross mountain rescue group and Statkraft.  
725 Lastly, we thank Statkraft for advising on weather conditions and NVE for their local avalanche forecasting.

## Competing interests

All co-authors other than EL declare that they have no conflict of interest. EL works for the hydropower company Statkraft, and Statkraft has an interest in the hydropower production at Austdalsbreen. Statkraft did not in any way influence the research objectives, data collection, analysis or interpretations of data presented in this paper.

## 730 Financial support

This study is a contribution to the JOSTICE project funded by the Norwegian Research Council (RCN grant #302458). In addition, the 2023 airborne survey was supported by funding from UH-nett Vest.

## References

- 735 Andreassen, Elvehøy, H., Kjøllmoen, B., Engeset, R. V. and Haakensen, N.: Glacier mass balance and length variation in Norway, *Ann. Glaciol.*, 42, 317–325, 10.3189/172756405781812826, 2005.
- Andreassen, L. M., Melvold, K., Nordli, Ø., Nordli, Ø., and Rasmussen, A.: Langfjordjøkelen, a rapidly shrinking glacier in northern Norway, *J. Glaciol.*, 58, 581–593, 10.3189/2012JoG11J014, 2012a.
- 740 Andreassen, L. M. and Winsvold, S. H. (eds), Paul, F. and Hausberg, J. E.: Inventory of Norwegian Glaciers, NVE report 38-2012. Norwegian Water Resources and Energy Directorate, Oslo, Norway, 2012b.
- Andreassen, L. M., Elvehøy, H., Huss, M., Melvold, K., and Winsvold, S. H.: Ice thickness measurements and volume estimates for glaciers in Norway, *J. Glaciol.*, 61, 763–775, 10.3189/2015JoG14J161, 2015.
- 745 Andreassen, L. M., Nagy, T., Kjøllmoen, B., and Leigh, J. R.: An inventory of Norway's glaciers and ice-marginal lakes from 2018–19 Sentinel-2 data, *J. Glaciol.*, 68, 2022.



- 750 Andreassen, L. M., Carrivick, J. L., Elvehøy, H., Kjøllmoen, B., Robson, B. A., and Sjrursen, K. H.: Spatio-temporal  
variability in geometry and geodetic mass balance of Jostedalbreen ice cap, Norway, *Ann. Glaciol.*, 1–18,  
10.1017/aog.2023.70, 2023.
- 755 Binder, D., Brückl, E., Roch, K. H., Behm, M., Schöner, W., and Hynek, B.: Determination of total ice volume and  
ice-thickness distribution of two glaciers in the Hohe Tauern region, Eastern Alps, from GPR data, *Ann. Glaciol.*,  
50, 71–79, 2009.
- Bolibar, J., Rabatel, A., Gouttevin, I., Zekollari, H., and Galiez, C.: Nonlinear sensitivity of glacier mass balance to  
future climate change unveiled by deep learning, *Nat. Commun.*, 13, 409, 2022.
- 760 Carrivick, J. L., Andreassen, L. M., Nesje, A., and Yde, J. C.: A reconstruction of Jostedalbreen during the Little  
Ice Age and geometric changes to outlet glaciers since then, *Quat. Sci. Rev.*, 284, 107501,  
<https://doi.org/10.1016/j.quascirev.2022.107501>, 2022.
- 765 Dowdeswell, J. A. and Evans, S.: Investigations of the form and flow of ice sheets and glaciers using radio-echo  
sounding, *Rep. Prog. Phys.*, 67, 1821, 10.1088/0034-4885/67/10/R03, 2004.
- Engen, S. H., Gjerde, M., Scheiber, T., Seier, G., Elvehøy, H., Abermann, J., Nesje, A., Winkler, S., Haualand, K.  
F., Rüter, D. C., Maschler, A., Robson, B. A., and Yde, J. C.: Investigation of the 2010 rock avalanche onto the  
regenerated glacier Brenndalsbreen, Norway, Submitted to *Landslides*, (accepted for publication).
- 770 Engeset, R. V., Jackson, M., and Schuler, T. V.: Analysis of the first jökulhlaup at Blåmannsisen, northern Norway,  
and implications for future events, *Ann. Glaciol.*, 42, 35–41, 10.3189/172756405781812600, 2005.
- 775 Farinotti, D., Huss, M., Bauder, A., Funk, M., and Truffer, M.: A method to estimate the ice volume and ice-thickness  
distribution of alpine glaciers, *J. Glaciol.*, 55, 422–430, 2009.
- 780 Farinotti, D., Brinkerhoff, D. J., Clarke, G. K. C., Fürst, J. J., Frey, H., Gantayat, P., Gillet-Chaulet, F., Girard, C.,  
Huss, M., Leclercq, P. W., Linsbauer, A., Machguth, H., Martin, C., Maussion, F., Morlighem, M., Mosbeux, C.,  
Pandit, A., Portmann, A., Rabatel, A., Ramsankaran, R., Reerink, T. J., Sanchez, O., Stenoft, P. A., Singh Kumari,  
S., van Pelt, W. J. J., Anderson, B., Benham, T., Binder, D., Dowdeswell, J. A., Fischer, A., Helfricht, K., Kutuzov,  
S., Lavrentiev, I., McNabb, R., Gudmundsson, G. H., Li, H., and Andreassen, L. M.: How accurate are estimates  
of glacier ice thickness? Results from ITMIX, the Ice Thickness Models Intercomparison eXperiment, *Cryosphere*,  
11, 949–970, 10.5194/tc-11-949-2017, 2017.
- 785 Farinotti, D., Huss, M., Fürst, J. J., Landmann, J., Machguth, H., Maussion, F., and Pandit, A.: A consensus  
estimate for the ice thickness distribution of all glaciers on Earth, *Nat. Geosci.*, 12, 168–173, 10.1038/s41561-019-  
0300-3, 2019.
- 790 Farinotti, D., Brinkerhoff, D. J., Fürst, J. J., Gantayat, P., Gillet-Chaulet, F., Huss, M., Leclercq, P. W., Maurer, H.,  
Morlighem, M., and Pandit, A.: Results from the ice thickness models intercomparison experiment phase 2  
(ITMIX2), *Front. Earth Sci.*, 8, 571923, 2021.
- 795 Fischer, A.: Calculation of glacier volume from sparse ice-thickness data, applied to Schaufelferner, Austria, *J.  
Glaciol.*, 55, 453–460, 10.3189/002214309788816740, 2009.
- Flowers, G. E. and Clarke, G. K. C.: Surface and bed topography of Trapridge Glacier, Yukon Territory, Canada:  
digital elevation models and derived hydraulic geometry, *J. Glaciol.*, 45, 165–174, 10.3189/S0022143000003142,  
1999.





- 800 Frank, T., van Pelt, W. J. J., and Kohler, J.: Reconciling ice dynamics and bed topography with a versatile and fast ice thickness inversion, *Cryosphere*, 17, 4021–4045, 10.5194/tc-17-4021-2023, 2023.
- Frank, T., and van Pelt, W. J. J.: Ice volume and thickness of all Scandinavian glaciers and ice caps, *J. Glaciol.*, 1–34, 10.1017/jog.2024.25, 2024.
- 805 Frémand, A. C., Fretwell, P., Bodart, J. A., Pritchard, H. D., Aitken, A., Bamber, J. L., Bell, R., Bianchi, C., Bingham, R. G., Blankenship, D. D., Casassa, G., Catania, G., Christianson, K., Conway, H., Corr, H. F. J., Cui, X., Damaske, D., Damm, V., Drews, R., Eagles, G., Eisen, O., Eisermann, H., Ferraccioli, F., Field, E., Forsberg, R., Franke, S., Fujita, S., Gim, Y., Goel, V., Gogineni, S. P., Greenbaum, J., Hills, B., Hindmarsh, R. C. A., Hoffman, A. O.,
- 810 Holmlund, P., Holschuh, N., Holt, J. W., Horlings, A. N., Humbert, A., Jacobel, R. W., Jansen, D., Jenkins, A., Jokat, W., Jordan, T., King, E., Kohler, J., Krabill, W., Kusk Gillespie, M., Langley, K., Lee, J., Leitchenkov, G., Leuschen, C., Luyendyk, B., MacGregor, J., MacKie, E., Matsuoka, K., Morlighem, M., Mouginot, J., Nitsche, F. O., Nogi, Y., Nost, O. A., Paden, J., Pattyn, F., Popov, S. V., Rignot, E., Rippin, D. M., Rivera, A., Roberts, J., Ross, N., Ruppel, A., Schroeder, D. M., Siegert, M. J., Smith, A. M., Steinhage, D., Studinger, M., Sun, B., Tabacco, I., Tinto, K.,
- 815 Urbini, S., Vaughan, D., Welch, B. C., Wilson, D. S., Young, D. A., and Zirizzotti, A.: Antarctic Bedmap data: Findable, Accessible, Interoperable, and Reusable (FAIR) sharing of 60 years of ice bed, surface, and thickness data, *Earth Syst. Sci. Data*, 15, 2695–2710, 10.5194/essd-15-2695-2023, 2023.
- Fürst, J. J., Gillet-Chaulet, F., Benham, T. J., Dowdeswell, J. A., Grabiec, M., Navarro, F., Pettersson, R., Moholdt, G., Nuth, C., and Sass, B.: Application of a two-step approach for mapping ice thickness to various glacier types on Svalbard, *Cryosphere*, 11, 2003–2032, 2017.
- 820 Gärtner-Roer, I., Naegeli, K., Huss, M., Knecht, T., Machguth, H., and Zemp, M.: A database of worldwide glacier thickness observations, *Glob. Planet. Change.*, 122, 330–344, <https://doi.org/10.1016/j.gloplacha.2014.09.003>,
- 825 2014.
- Giesen, R. H. and Oerlemans, J.: Response of the ice cap Hardangerjøkulen in southern Norway to the 20th and 21st century climates, *Cryosphere*, 4, 191–213, 10.5194/tc-4-191-2010, 2010.
- 830 Gillespie, M. K., Yde, J. C., Andresen, M. S., Citterio, M., and Gillespie, M. A. K.: Ice geometry and thermal regime of Lyngmarksbræen Ice Cap, West Greenland, *J. Glaciol.*, 1–13, 10.1017/jog.2023.89, 2023.
- Gillespie, M. K., Andreassen, L. M., Huss, M., de Villiers, S., Sjursen, K. H., Aasen, J., Bakke, J., Cederstrøm, J. M., Elvehøy, H., Kjølmoen, B., Loe, E., Meland, M., Melvold, K., Nerhus, S. D., Røthe, T. O., Støren, E. W. N., Øst, K., and Yde, J. C.: Jostedalbreen ice thickness and bed topography [dataset], 10.58059/yhwr-rx55, 2024.
- 835 GlaThiDa Consortium: Glacier Thickness Database 3.1.0, <https://doi.org/10.5904/wgms-glathida-2020-10>, 2020.
- Glen, J. W.: The creep of polycrystalline ice, *Proceedings of the Royal Society of London. Series A. Mathematical and Physical Sciences*, 228, 519–538, 1955.
- 840 Grab, M., Mattea, E., Bauder, A., Huss, M., Rabenstein, L., Hodel, E., Linsbauer, A., Langhammer, L., Schmid, L., and Church, G.: Ice thickness distribution of all Swiss glaciers based on extended ground-penetrating radar data and glaciological modeling, *J. Glaciol.*, 67, 1074–1092, 2021.
- 845 Huss, M. and Farinotti, D.: Distributed ice thickness and volume of all glaciers around the globe, *J. Geophys. Res. Earth Surf.*, 117, 2012.



- 850 Huss, M. and Farinotti, D.: A high-resolution bedrock map for the Antarctic Peninsula, *Cryosphere*, 8, 1261–1273, 2014.
- Haakensen, N. and Wold, B.: Breheimen-Stryn: Undersøkelse av bunntopografi på Bødalsbreen, *NVE Rapp.*, 17–86, 1986.
- 855 IPCC: *Climate Change 2021: The Physical Science Basis. Contribution of Working Group I to the Sixth Assessment Report of the Intergovernmental Panel on Climate Change*, 2021.
- Johansson, F. E., Bakke, J., Støren, E. N., Gillespie, M. K., and Laumann, T.: Mapping of the Subglacial Topography of Folgefonna Ice Cap in Western Norway—Consequences for Ice Retreat Patterns and Hydrological Changes, *Front. Earth Sci.*, 10, 10.3389/feart.2022.886361, 2022.
- 860 Kennett M.: Kartlegging av istykkelse og feltavgrensning på Spørteggbreen 1989, *NVE Rapp.* 15-1989, oppdragsrapport1989\_15.pdf (nve.no), 1989.
- 865 Kennett M.: Kartlegging av istykkelse og feltavgrensning på Blåmannsisen 1990, *NVE Rapp.* 8-1990 oppdragsrapport1990\_08.pdf (nve.no), 1990.
- Kjøllmoen, B., Andreassen, L.M. and Elvehøy H.: *Glaciological investigations in Norway 2023; NVE Rapp.* xx-2024, in prep.
- 870 Lapazaran, J. J., Martín-Español, A., Navarro, F. J., and Otero, J.: On the errors involved in ice-thickness estimates I: ground-penetrating radar measurement errors, *J. Glaciol.*, 62, 1008–1020, 10.1017/jog.2016.93, 2016.
- Laumann, T. and Nesje, A.: The impact of climate change on future frontal variations of Briksdalsbreen, western Norway, *J. Glaciol.*, 55, 789–796, 10.3189/002214309790152366, 2009.
- 875 Laumann, T. and Nesje, A.: Spørteggbreen, western Norway, in the past, present and future: Simulations with a two-dimensional dynamical glacier model, *Holocene*, 24, 842–852, 10.1177/0959683614530446, 2014.
- 880 Lindbäck, K., Kohler, J., Pettersson, R., Nuth, C., Langley, K., Messerli, A., Vallot, D., Matsuoka, K., and Brandt, O.: Subglacial topography, ice thickness, and bathymetry of Kongsfjorden, northwestern Svalbard, *Earth Syst. Sci. Data*, 10, 1769–1781, 10.5194/essd-10-1769-2018, 2018.
- 885 Linsbauer, A., Paul, F., and Haeberli, W.: Modeling glacier thickness distribution and bed topography over entire mountain ranges with GlabTop: Application of a fast and robust approach, *J. Geophys. Res. Earth Surf.*, 117, 2012.
- Millan, R., Mougnot, J., Rabatel, A., and Morlighem, M.: Ice velocity and thickness of the world’s glaciers, *Nat. Geosci.*, 15, 124–129, 10.1038/s41561-021-00885-z, 2022.
- 890 Mingo, L. and Flowers, G. E.: An integrated lightweight ice-penetrating radar system, *J. Glaciol.*, 56, 709–714, 10.3189/002214310793146179, 2010.
- Morlighem, M., Williams, C. N., Rignot, E., An, L., Arndt, J. E., Bamber, J. L., Catania, G., Chauché, N., Dowdeswell, J. A., Dorschel, B., Fenty, I., Hogan, K., Howat, I., Hubbard, A., Jakobsson, M., Jordan, T. M., Kjeldsen, K. K., Millan, R., Mayer, L., Mougnot, J., Noël, B. P. Y., O’Cofaigh, C., Palmer, S., Rysgaard, S., Seroussi, H., Siegert, M. J., Slabon, P., Straneo, F., van den Broeke, M. R., Weinrebe, W., Wood, M. and Zinglarsen, K. B.: *BedMachine v3: Complete bed topography and ocean bathymetry mapping of Greenland from multibeam echo sounding combined with mass conservation*, *Geophys. Res. Lett.*, 44, 11,051–11,061. 10.1002/2017GL074954, 2017.



- 900 Navarro, F. and Eisen, O.: Ground-penetrating radar in glaciological applications, in: Remote sensing of glaciers: Techniques for topographic, spatial and thematic mapping of glaciers, Taylor & Francis London, 195–229, 2009.
- Nesje, A., Johannessen, T., and Birks, H. J. B.: Brikisdalsbreen, western Norway: climatic effects on the terminal response of a temperate glacier between AD 1901 and 1994, *Holocene*, 5, 343–347,  
905 10.1177/095968369500500310, 1995.
- Ogier, C., van Manen, D.-J., Maurer, H., Räss, L., Hertrich, M., Bauder, A., and Farinotti, D.: Ground penetrating radar in temperate ice: englacial water inclusions as limiting factor for data interpretation, *J. Glaciol.*, 1–12, 2023.
- 910 Pettersson, R., Christoffersen, P., Dowdeswell, J. A., Pohjola, V. A., Hubbard, A., and Strozzi, T.: Ice thickness and basal conditions of Vestfonna ice cap, eastern Svalbard, *Geogr. Ann. A: Phys. Geogr.*, 93, 311–322, 2011.
- Plewes, L. A. and Hubbard, B.: A review of the use of radio-echo sounding in glaciology, *Prog. Phys. Geogr.*, 25, 203–236, 2001.
- 915 Rounce, D. R., Hock, R., Maussion, F., Hugonnet, R., Kochtitzky, W., Huss, M., Berthier, E., Brinkerhoff, D., Compagno, L., and Copland, L.: Global glacier change in the 21st century: Every increase in temperature matters, *Science*, 379, 78–83, 2023.
- 920 Schlegel, R., Kulesa, B., Murray, T., and Eisen, O.: Towards a common terminology in radioglaciology, *Ann. Glaciol.*, 63, 8–12, 2022.
- Seier, G., Abermann, J., Andreassen, L. M., Carrivick, J. L., Kielland, P. H., Löffler, K., Nesje, A., Robson, B. A., Røthe, T. O., Scheiber, T., Winkler, S. and Yde, J. C.: Glacier thinning, recession and advance, and the associated evolution of a glacial lake between 1966 and 2021 at Austerdalsbreen, western Norway, *Land. Degrad. Dev.*, 2024.
- Sellevoid, M. and Kloster, K.: Seismic measurements on the glacier Hardangerjøkulen, Western Norway, *Nor. Polarinst. Årb.*, 87–91, 1964.
- 930 Smith, B. E. and Evans, S.: Radio echo sounding: absorption and scattering by water inclusion and ice lenses, *J. Glaciol.*, 11, 133–146, 1972.
- Sverrisson, M., Jóhannesson, Æ., and Björnsson, H.: Instruments and Methods: Radio-Echo Equipment for Depth Sounding of Temperate Glaciers, *J. Glaciol.*, 25, 477–486, 1980.
- 935 Sætrang, A. C.: Istykkelsesmålinger med breradar på Austdalsbreen, *Heli-Anlegg Rapp.*, 5–88, 1988.
- Sætrang, A. C. and Holmqvist, E.: Kartlegging av istykkelse på nordre Jostedalsbreen, *NVE Rapp.*, 8-1987, 1987.
- 940 Sætrang, A. C. and Wold, B.: Results from the radio echo-sounding on parts of the Jostedalsbreen ice cap, Norway, *Ann. Glaciol.*, 8, 156–158, 1986.
- Terratec: Laserskanning for nasjonal detaljert høydemodell, NDH Jostedalsbreen 2pkt, 2020.
- 945 Welty, E., Zemp, M., Navarro, F., Huss, M., Fürst, J. J., Gärtner-Roer, I., Landmann, J., Machguth, H., Naegeli, K., and Andreassen, L. M.: Worldwide version-controlled database of glacier thickness observations, *Earth Syst. Sci. Data.*, 12, 3039–3055, 2020.



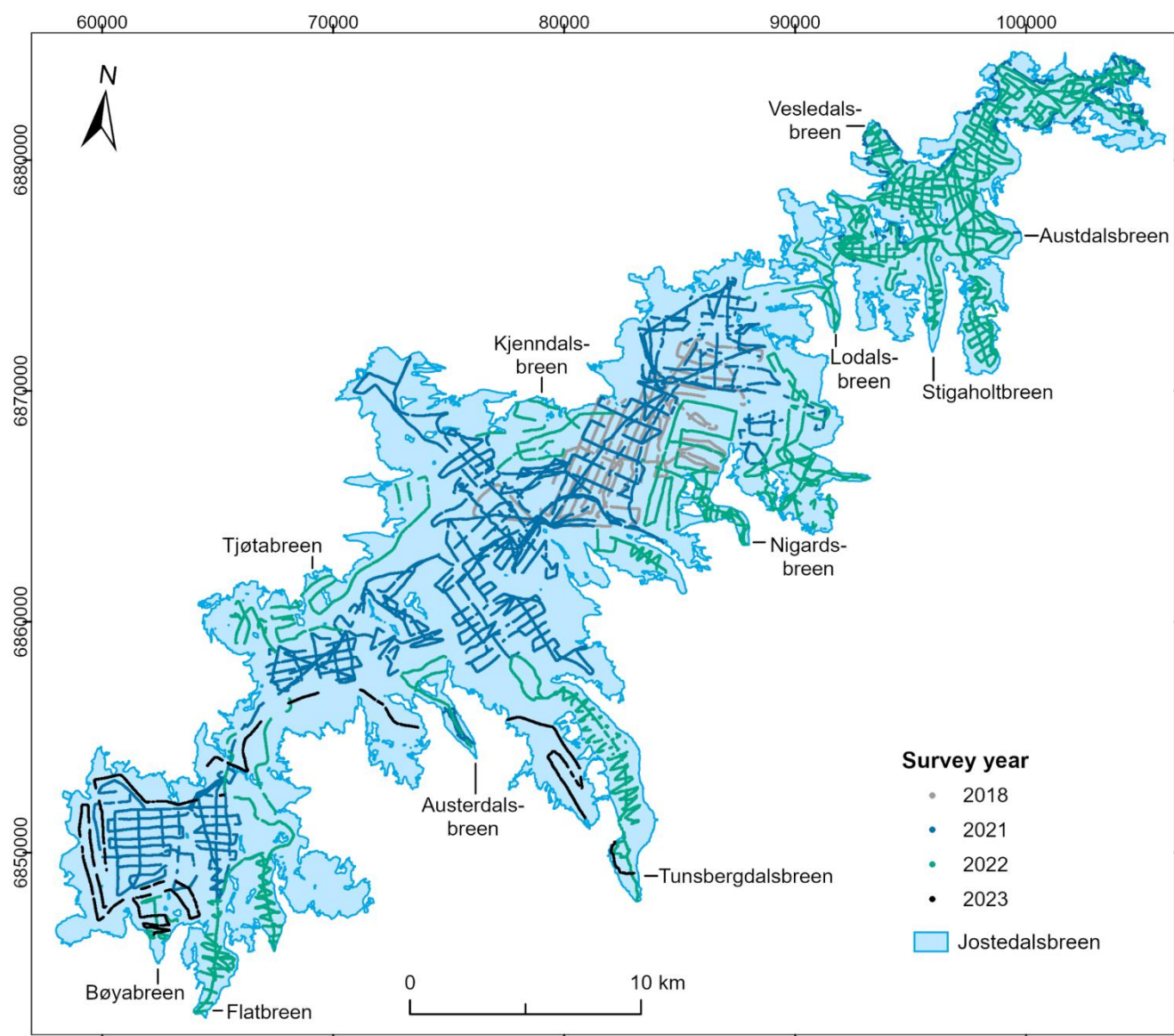
- 950 Yde, J. C., Gillespie, M. K., Løland, R., Ruud, H., Mernild, S. H., Villiers, S. D., Knudsen, N. T., and Malmros, J. K.: Volume measurements of Mittivakkat Gletscher, southeast Greenland, *J. Glaciol.*, 60, 1199–1207, 2014.
- Østrem, G., Liestøl, O., and Wold, B.: Glaciological investigations at Nigardsbreen, Norway, *Nor. Geogr. Tidsskr.*, 30, 187–209, 10.1080/00291957608552005, 1976.
- 955 Åkesson, H., Nisancioglu, K. H., Giesen, R. H., and Morlighem, M.: Simulating the evolution of Hardangerjøkulen ice cap in southern Norway since the mid-Holocene and its sensitivity to climate change, *Cryosphere*, 11, 281–302, 2017.



960

## Appendices

### Appendix A



965

**Figure A1:** Locations of ice thickness measurements divided into survey year. The coordinate system is UTM 33N, datum ETRS89.



## Appendix B

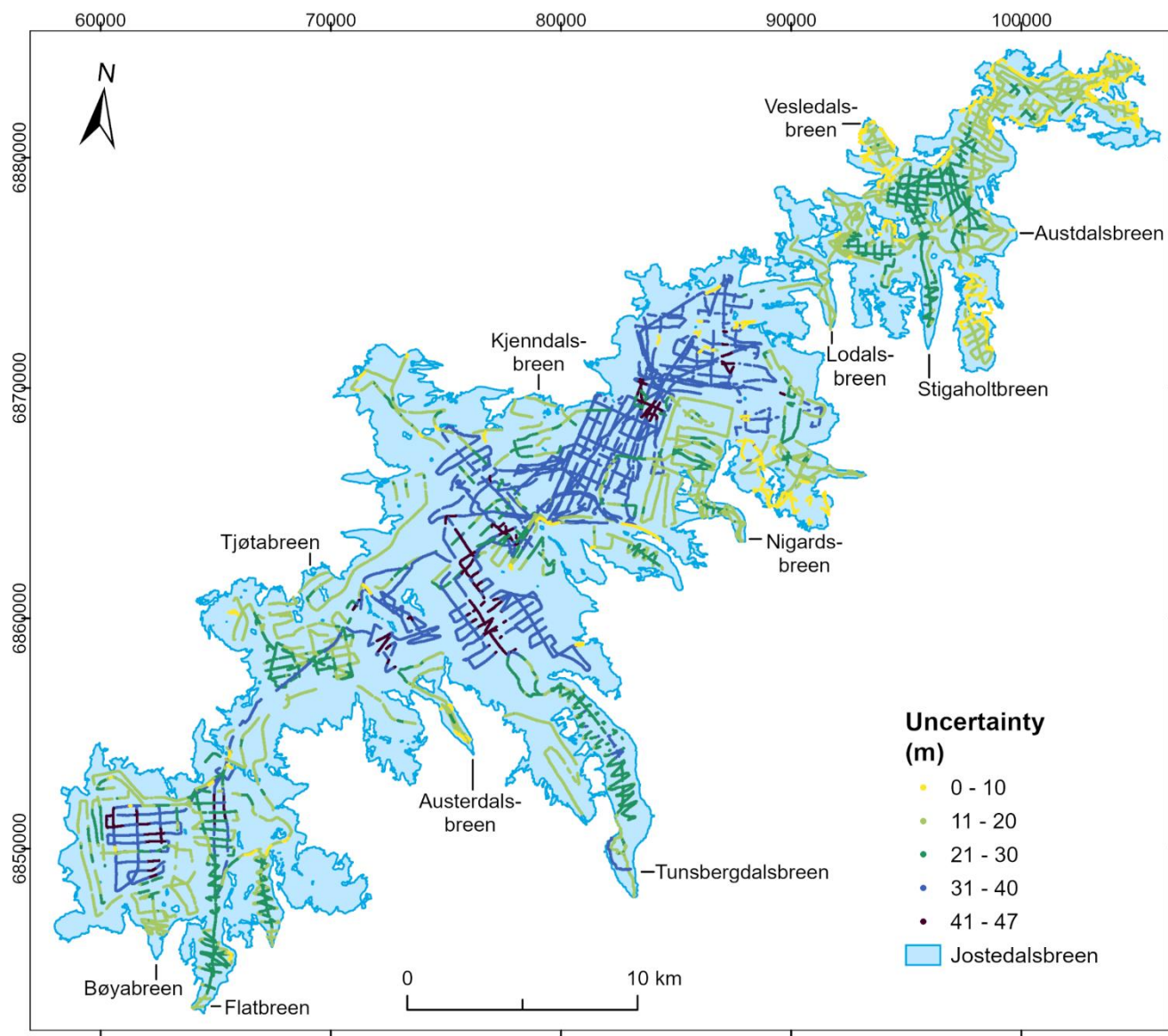


**Figure B1:** Total measurement uncertainty associated with each ice thickness observation calculated using the method described by Lapazaran et al. (2016). The coordinate system is UTM 33N, datum ETRS89.